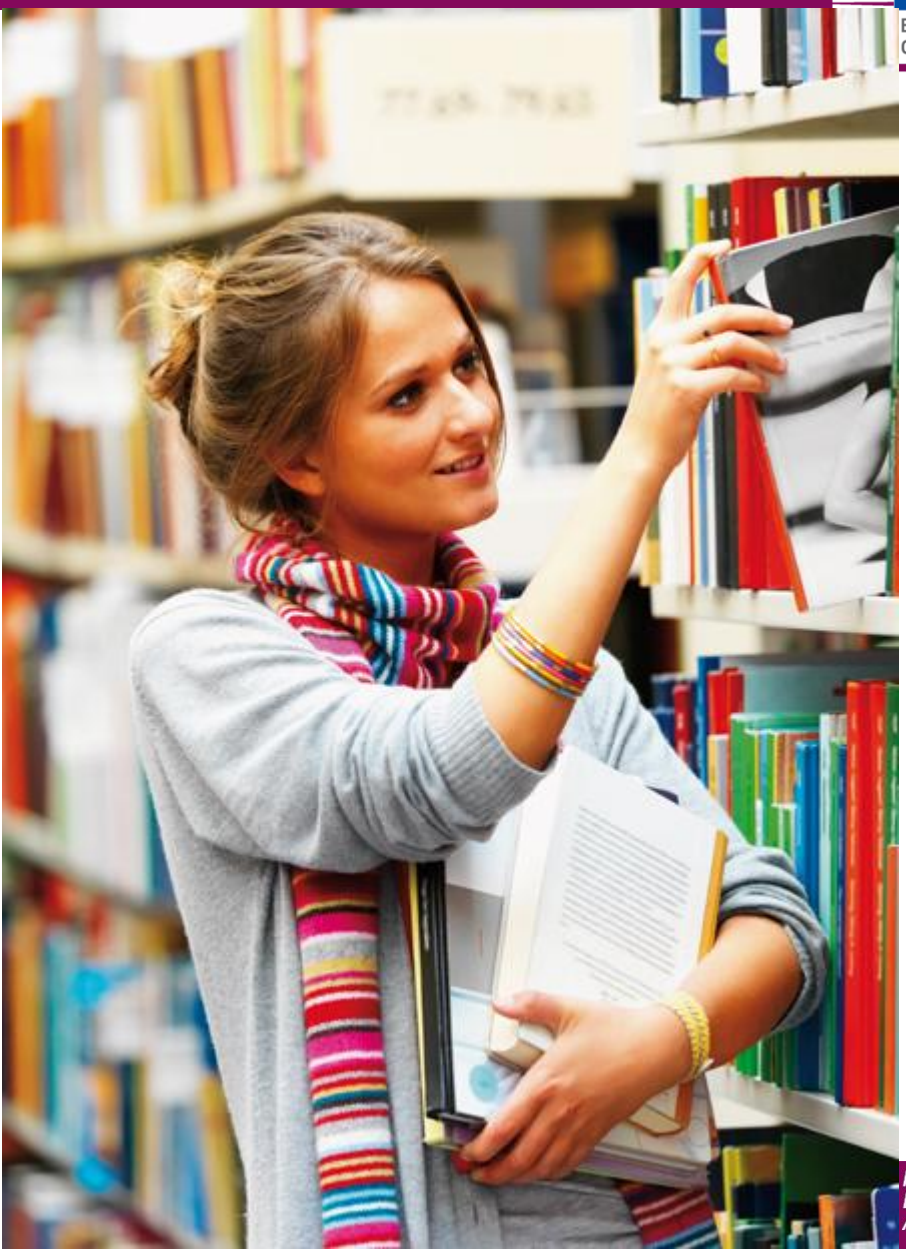

European Commission

Research Executive Agency

H2020 Marie Skłodowska-Curie Actions

Fracture in fibre-reinforced thermoplastics across the scales

Juan M Macías López

Fracture in fibre-reinforced thermoplastics across the scales

Juan M Macías López

Supervisors:

Fermín Otero
Pedro Camanho
Albertino Arteiro
José Reinoso

H2020 Marie Skłodowska-Curie Actions
Newfrac

European Commission

Outline

- Introduction
- Phase Field Method
- Micromechanical analysis of composite materials
- Phase-Field implementation
- Single fibre analysis
- RVE analysis
- Embedded cell models
- Conclusions and future work

Introduction

Research Executive Agency

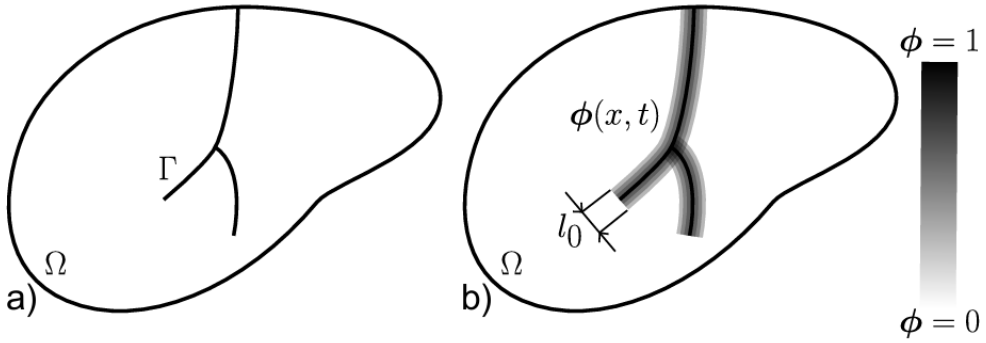

Fig. 2.1 Schematic representation of a solid body with (a) an internal discrete discontinuity, and (b) a Phase-Field approximation of the same discontinuity [1,2].

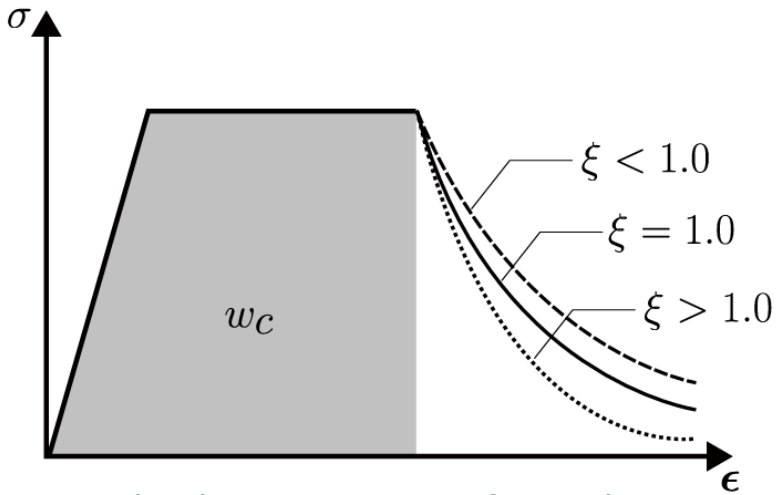

Fig 3.1 Graphical representation of w_c and ξ parameters in the PF formulation of Miehe et al. [4].

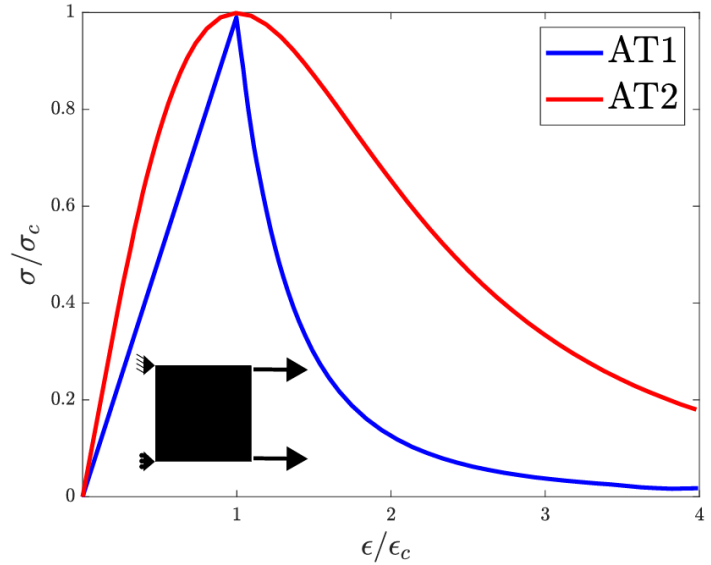

Fig. 2.2 Stress-strain behaviour for AT1 and AT2 models in a single finite element under tension [3], where σ_c is the strength and ϵ_c is the strain when the stress reaches σ_c .

Introduction (Chapter 1)

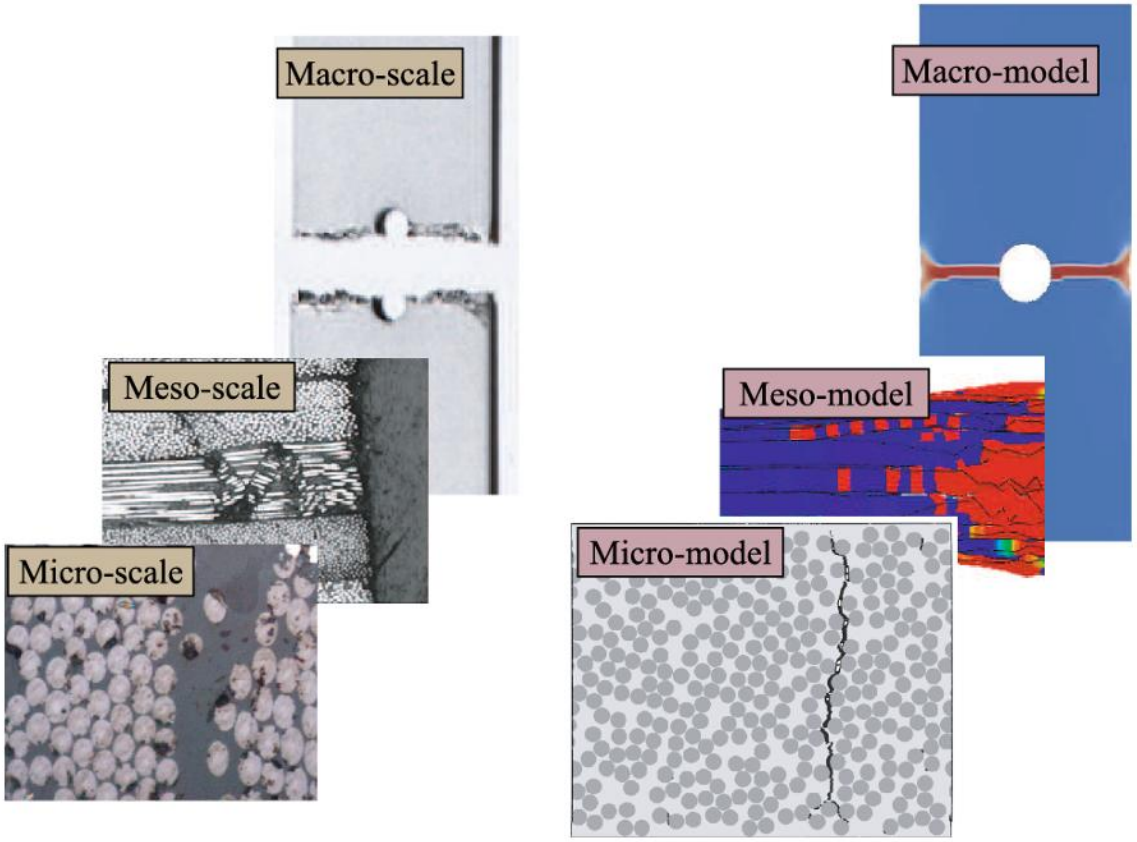

Fig 4.1: Modelling damage in composite materials at different scales [5]. *Reprinted by per mission from Springer Nature: Archives of Computational Methods in Engineering, Simulation of the Mechanical Response of Thin-Ply Composites: From Computational Micro-Mechanics to Structural Analysis, Albertino Arteiro et al, Copyright (2019).*

Research questions

- What are the main reasons for the large differences in the available values of material properties and how can one sort realist values out of such disperse pool of information?
- Is the current experimental data reliable to perform calibration/validation of material models used to approximate local micro-scale fields?
- How accurate are the current PF formulations to predict micro-scale fracture phenomena on UD FRPs, incl. thermoplastic-based composites, if realistic geometric dimensions and material properties are taken into account?
- What are the dimensions and boundary conditions in an RVE analysis necessary to accurately capture micro-scale fracture phenomena using PF?

Objectives

European Commission

- Understand the current state-of-the-art, regarding numerical and experimental techniques used to study micro-scale fracture in UD FRPs, incl. FRTPs.
- Understand the capabilities and limitations of current Phase-Field formulations for the micro-scale analysis of UD FRPs, incl. FRTPs, using RVE analysis and embedded cell models.

Phase Field Method

Phase-Field method

Fig. 2.1 Schematic representation of a solid body with (a) an internal discrete discontinuity, and (b) a Phase-Field approximation of the same discontinuity [1,2].

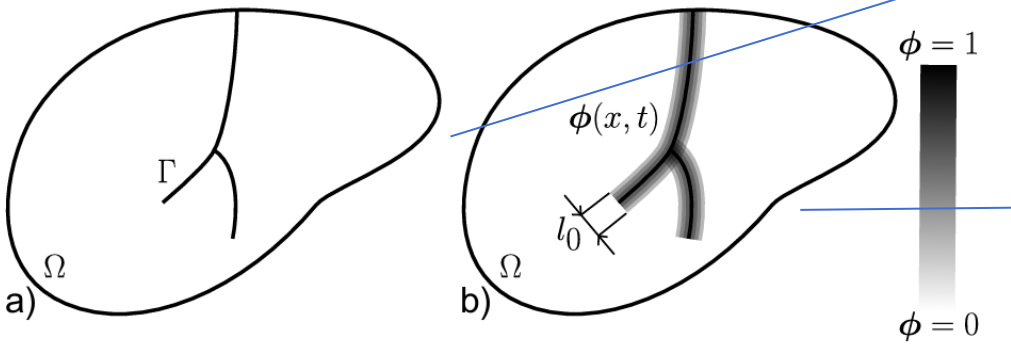

Variational form of the Griffith thermodynamic balance [1,2].

$$\Pi(\mathbf{u}) = \int_\Omega \Psi_0(\mathbf{u})\mathrm{d}\Omega + \int_\Gamma G_c \mathrm{d}S - W_{ext}(\mathbf{u})$$

$$\Pi(\mathbf{u}) \approx \Pi(\mathbf{u},\phi)$$

$$\Pi(\mathbf{u},\phi) = \int_\Omega \Psi(\mathbf{u},\phi)\mathrm{d}\Omega + \int_\Omega \frac{G_c}{4C_w}\gamma(\phi;\nabla\phi)\mathrm{d}\Omega - W_{ext}(\mathbf{u})$$

$$\int_\Omega \left[g(\phi)\Psi^+(\mathbf{u}) + \Psi^-(\mathbf{u})\right]\mathrm{d}\Omega$$

Energy degradation function [1,2].

$$\frac{G_c}{4C_w}\int_\Omega \left(\frac{\alpha(\phi)}{l_0} + l_0|\nabla\phi|^2\right)\mathrm{d}\Omega$$

Geometric crack function [1,2].

Micromechanical analysis of composite materials

Single fibre models

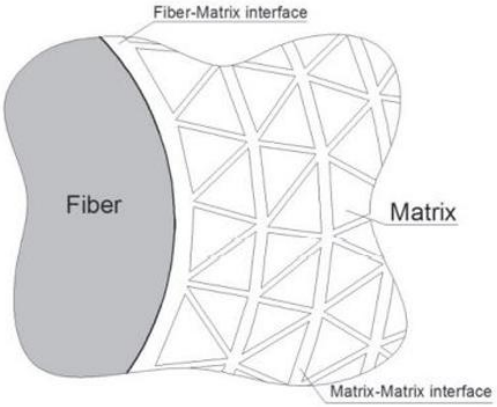

Fig 4.5: Cohesive damage modelling for interface and matrix cracking [7]. *No permission is required for the reprint of this figure.*

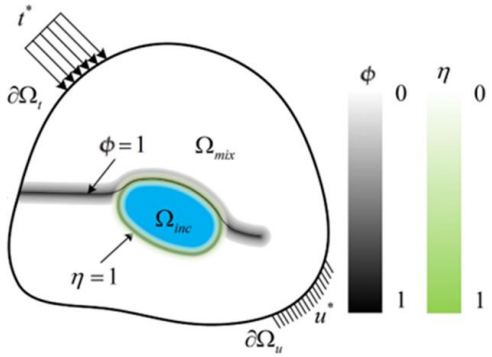

Fig 4.6: Diffuse interface (η) and damage (φ) representation [8]. *Reprinted from Modelling progressive failure in multi-phase materials using a phase field method, PengZhang, Xiaofei Hu, Shangtong Yang, Weian Yao, Pages No. 107, Copyright (2019), with permission from Elsevier*

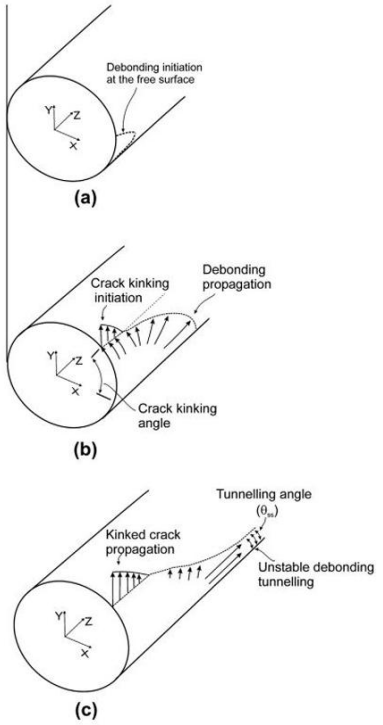

Fig 4.4: Failure sequence in a single embedded fibre: a) Debonding initiation, b) interface fracture propagation and kinking, and c) kinking propagation and tunnelling [6]. *Reprinted from 3D in situ observations of glass fibre/matrix interfacial debonding, Karolina Martyniuka, Bent F., Sørensena, Peter Modreggerbc, Erik M.Lauridsen, Pages No. 71, Copyright (2013), with permission from Elsevier.*

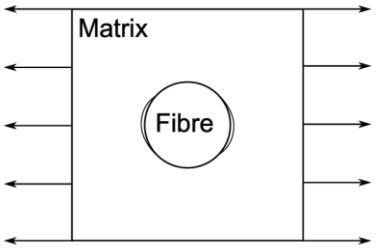

Fig 4.2: Single fibre modelling approach.

Representative Volume Element (RVE) analysis

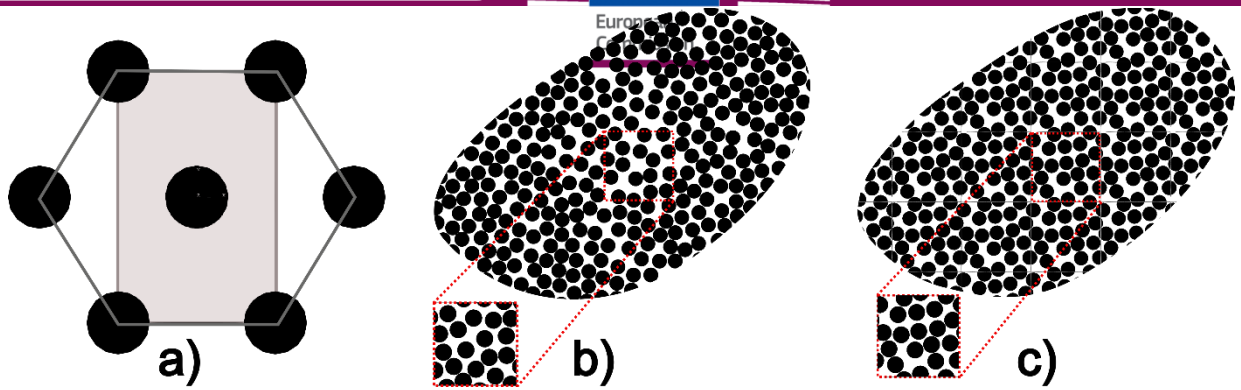

Fig 4.8: a) RVE with a hexagonal fibre distribution [12], b) non-periodic RVE with a random fibre distribution [13], and c) periodic RVE with a random fibre distribution.

- In the work of Nguyen et al. [114] the term RVE is replaced by "statistical microstructural volume elements" (SMVE) which is not restricted by the periodic arrangement (see Fig. 4.8 b)).
- In the work of Wu et al. [44] the term RVE is replaced by the terminology "Stochastic Volume Elements" (SVEs).
- The work of Bai et al. [116] mentions Statistical Volume Elements (SVEs) and RVEs. In [116], the definitions are linked to the unit cell size.

Statistical definition

- The work of Pulungan et al. [115] refers to RVEs of random, square and hexagonal fibre patterns (see Fig. 4.8 a)).
- In the work of Arteiro et al. [83] the term RVE refers to sections of an embedded cell model for a cross-ply laminate analysis, where periodicity is assumed in the longitudinal direction.
- In the work of Naya et al. [82], one analysis is performed on a single-fibre model called “single-fibre RVE.”

Mechanical definition

Embedded cell models

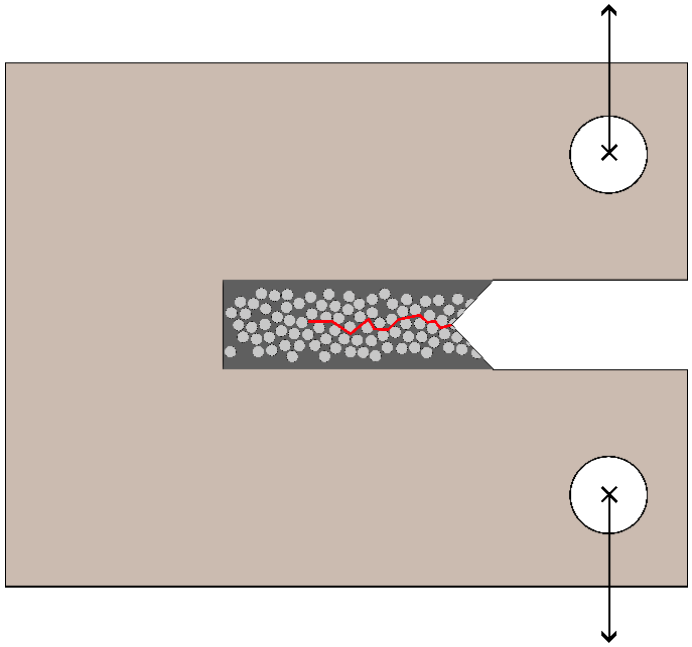

Fig 4.3: Schematic of an embedded cell simulation of fracture.

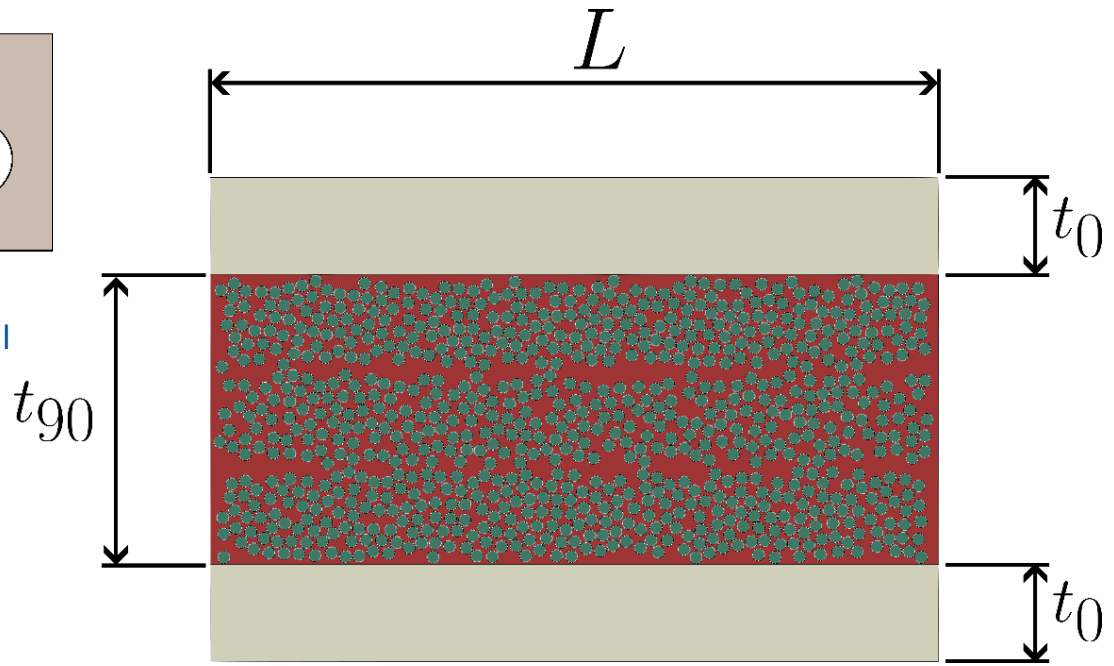

Fig 4.10: Relation between laminate length L, 0-degree ply thickness t_0, and 90-degree ply thickness t_{90}.

Embedded cell models

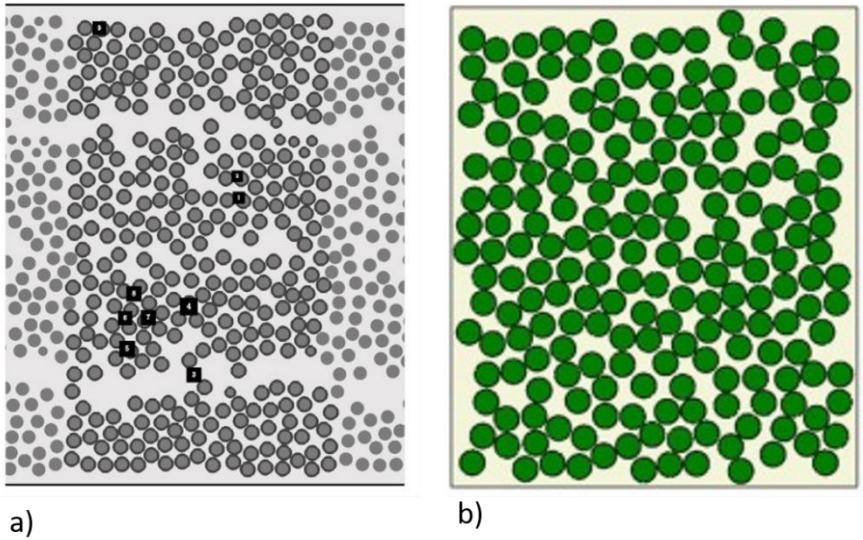

Fig 4.9: Comparison of micro-scale fibre distributions: a) generated from micro-graphs [14] *(Reprinted from Micromechanical analysis of damage mechanisms under tension of 0°–90° thin ply composite laminates, M.Naderi, N.Iyyer, Pages No. 2, Copyright (2020), with permission from Elsevier), b) artificially generated [15] (Reprinted from In-situ strength effects in long fibre reinforced composites: A micro-mechanical analysis using the phase field approach of fracture, T.Guillén-Hernández, A.Quintana-Corominas, I.G.Garcíac, J.Reinosoc, M.Paggi, A.Turón, Pages No. 10, Copyright (2020), with permission from Elsevier).*

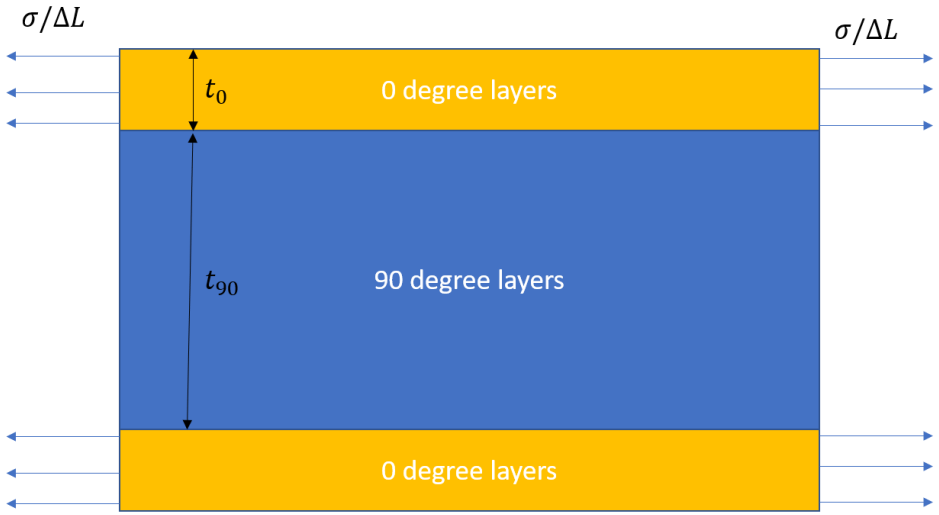

Fig 4.14: Different boundary conditions in embedded cell models.

Constitutive models, interactions and material properties

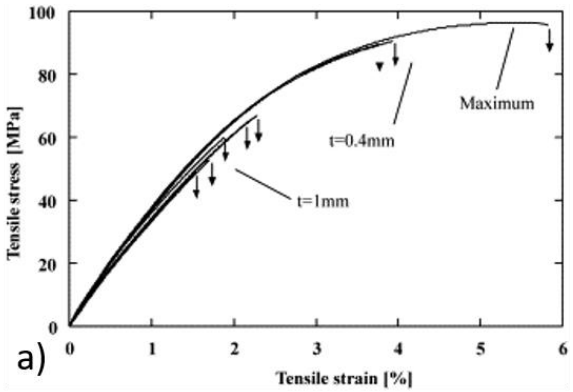

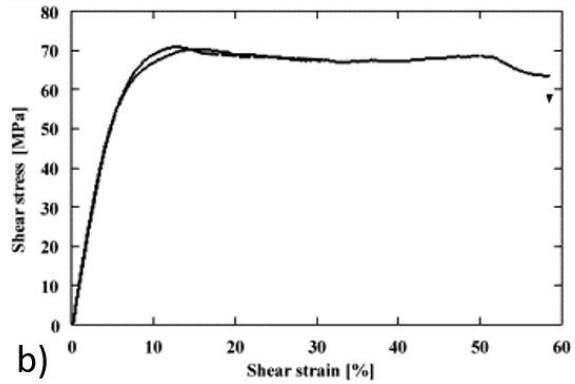

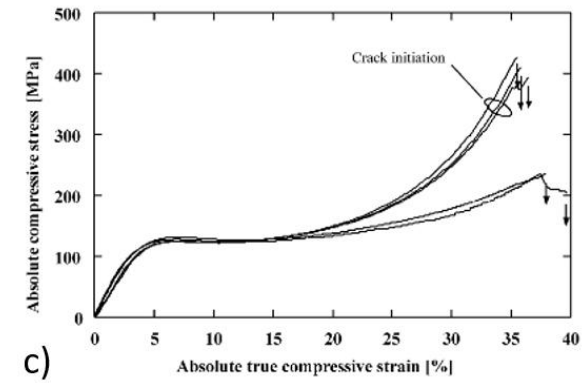

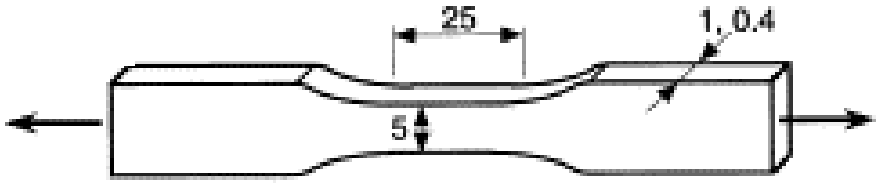

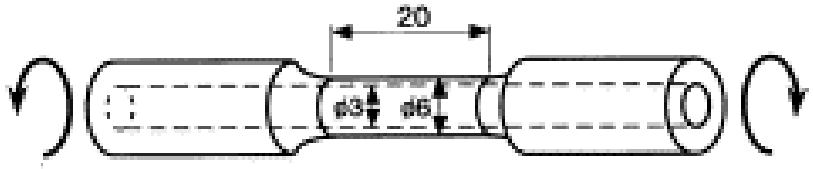

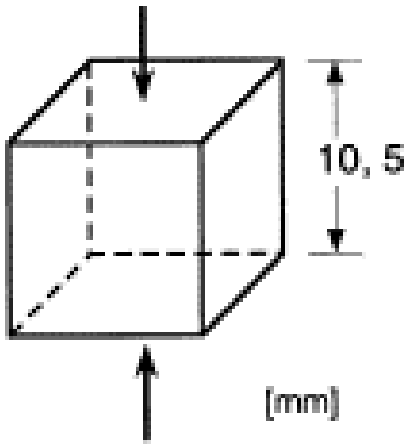

Fig 4.11/13: Representative stress/true strain curves and specimens for a) tensile test, b) shear test and c) com pressive test [16]. *Reprinted from Failure behavior of an epoxy matrix under different kinds of static loading, B Fiedler, M Hojo, S Ochiai, K Schulteb, M Ando, Pages No. 1617, 1618, 1619, Copyright (2001), with permission from Elsevier*

European Commission

Research Executive Agency

Source/ internal reference	Material type	Tensile strength [MPa]	Compressive strength [MPa]	Fracture toughness [N/mm]
Melro et al. [46] From Fiedler et al. [16]	Hexcel 6376 (epoxy)	93	124	0.09
Vaughan and McCarthy [119] From Fiedler et al. [16]	Hexcel 6376 (epoxy)	103	264	–
Naya et al. [126] From Herraez et al. [158]	Hexcel 8552 (epoxy)	121	176	0.1
Pineda et al. [138] From calibration	MY750/HY917/DY063 (epoxy)	66.5	–	0.000563
Chevalier et al. [106] Morelle [165]	RTM6 (epoxy)	–	–	0.001
Song et al. [132] From calibration	Solvalite 710-1 (epoxy)	–	550	–
Labanda et al. [7] –	Epoxy	50	–	0.5
Kohler et al. [151] –	Toray TP80ep (epoxy)	–	–	0.064
Tan and Martínez-Pañeda [28] –	Epoxy	20	–	0.01
Arteiro et al. [83] From Fiedler et al. [16]	Toho #113 (epoxy)	93	350	0.277

Table 4.3: Matrix mechanical properties based on different publications.

Source	Materials type	Normal strength [MPa]	Shear strength [MPa]	G_{IC} [N/mm]	G_{IIC} [N/mm]
[46]	Glass/Epoxy	50	70	0.002	0.006
[28]	Glass/Epoxy	40	60	0.125	0.15
[122]	Glass/Epoxy	10	40	0.025	0.1
[121]	Carbon/Epoxy	100	–	0.1	–
[126]	Carbon/Epoxy	42	64	0.002	0.1
[106]	Carbon/Epoxy	50	75	0.002	0.006
[158]	Carbon/Epoxy	100	75	0.01	0.01

Table 4.4: Interface mechanical properties based on different publications.

Phase-Field implementation

Phase-Field implementation

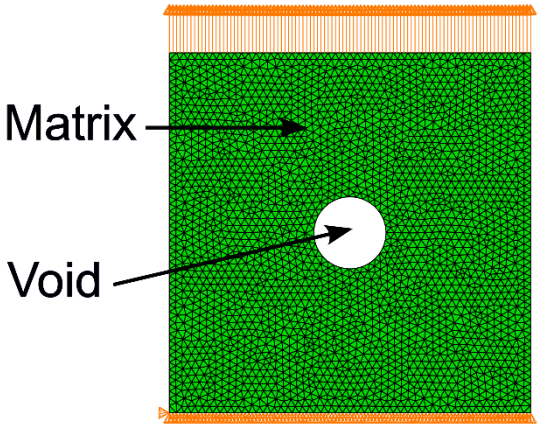

Fig 5.1: Mesh and BC for the open-hole specimen under tensile loading.

Matrix			
E [MPa]	ν [-]	l_0 [μm]	G_c [N/mm]
3760	0.39	1.0	0.02
Fibre			
E [MPa]	ν [-]	l_0 [μm]	G_c [N/mm]
1500	0.2	[-]	[-]
Interface			
K_I [N/mm^3]	K_{II} [N/mm^3]	σ_{I0} [MPa]	σ_{II0} [MPa]
10^8	10^8	50.0	75.0
G_{Ic} [N/mm]	G_{IIc} [N/mm]	BK law [-]	
0.002	0.006	1.45	

Table 5.1: Material properties for fibre, matrix and fibre-matrix interface used in linear elastic AT1 and AT2 formulations for micro-mechanical numerical tests [18].

Implementation	Total number of iterations	Running time
UEL Newton-Raphson	515	00 : 18 : 00
UEL Quasi-Newton	557	00 : 15 : 00
UMAT-Thermal	593	01 : 06 : 00

Table 5.2: Comparison of total number of iterations and running time for the model in Fig. 5.1 using a UEL with a standard Newton-Raphson scheme, a UEL with a Quasi-Newton scheme and a UMAT-Thermal implementation.

Open-Hole specimen

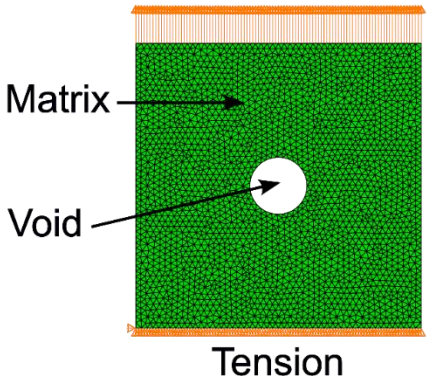

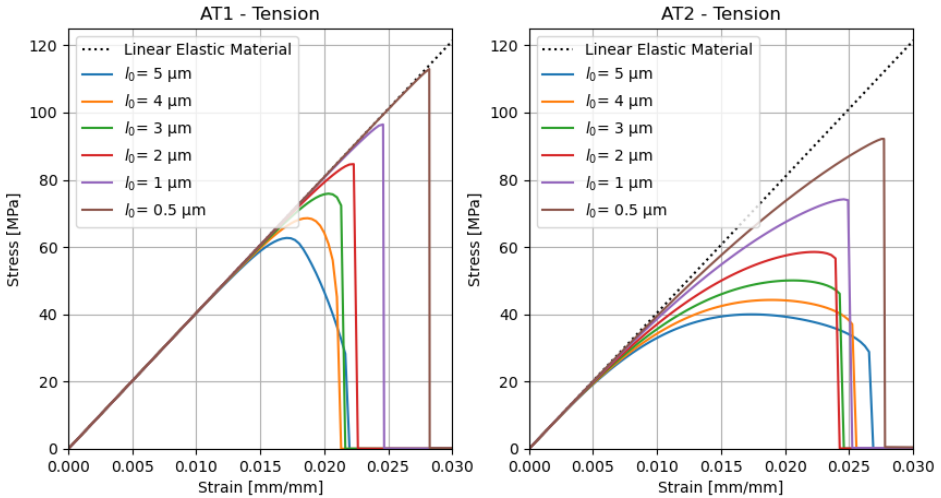

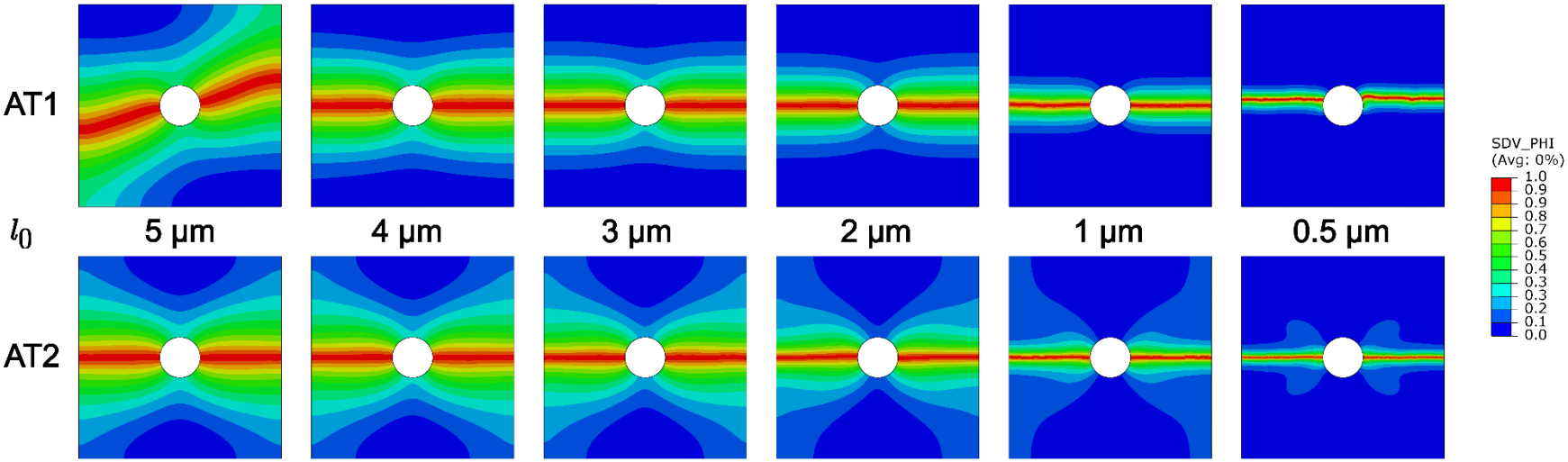

Fig 5.8: Crack patterns for AT1 and AT2 formulations under tensile loading and different values of the length scale parameter.

Open-Hole specimen

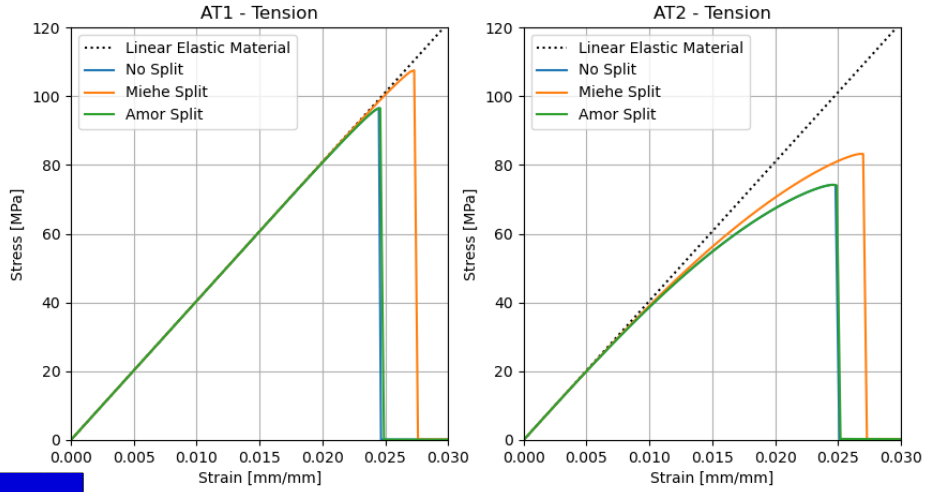

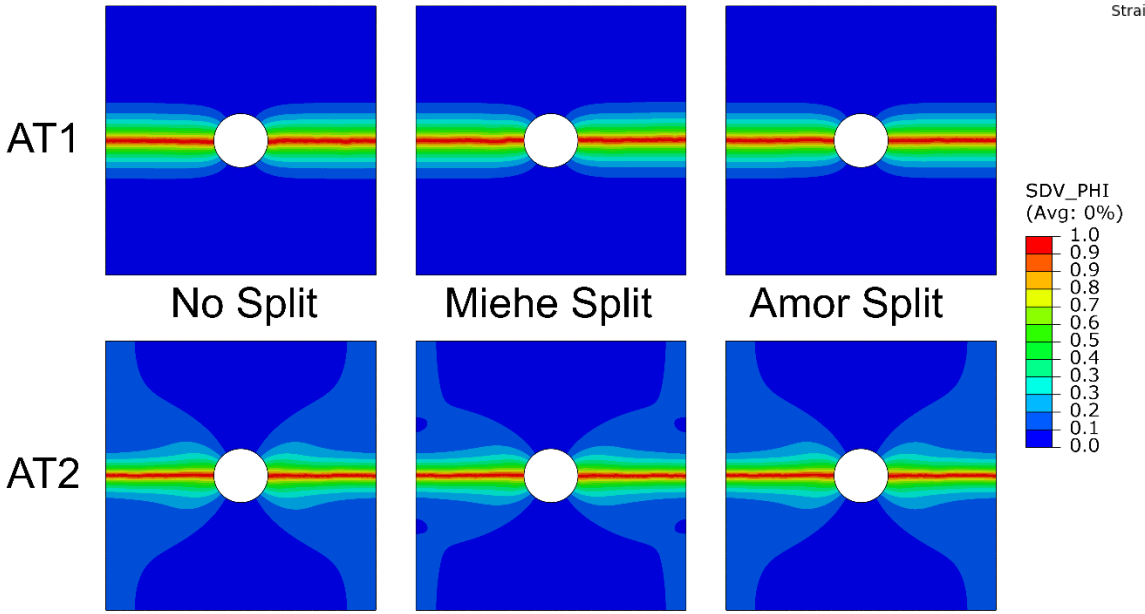

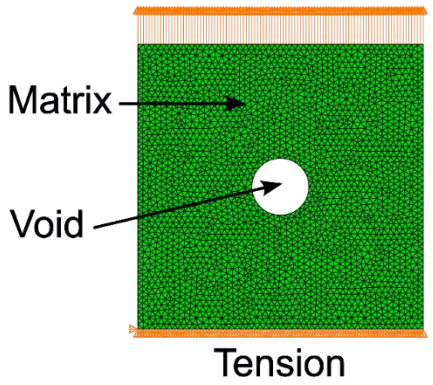

Fig 5.14: Crack patterns for AT1 and AT2 formulations under tensile loading and different energy splits.

Research Executive Agency

Single fibre analysis

Single fibre (Cohesive damage)

Fig 6.6: Cohesive damage distribution around the fibre at 0.015 strain, for the models considering cohesive interface damage for different values of cohesive strength and cohesive fracture toughness for the single-fibre specimen.

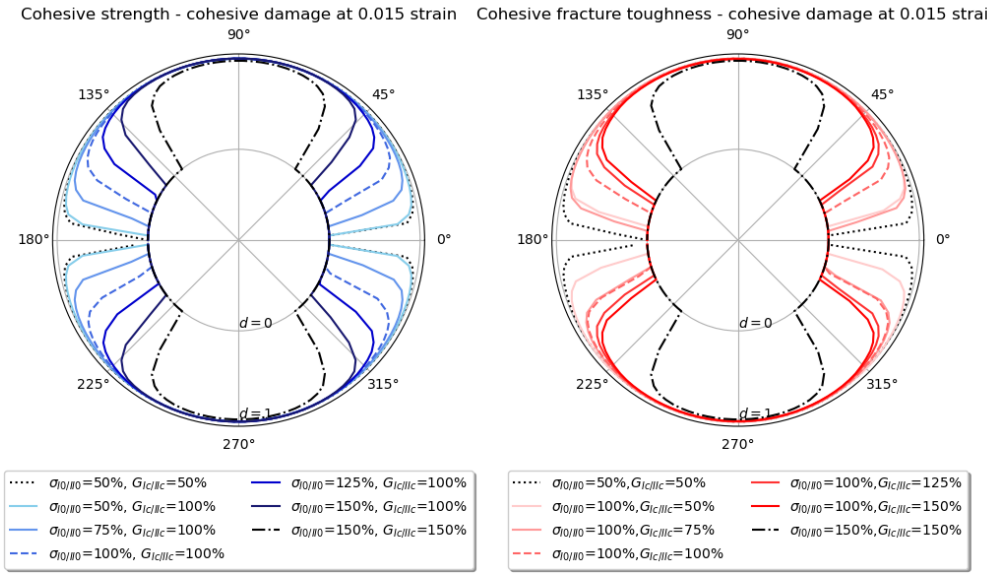

Fig 6.5: Stress-strain curves and cohesive damage distribution around the fibre for a perfect interface connection compared to models considering a damageable cohesive interface with different values of cohesive strength and cohesive fracture toughness for the single-fibre specimen.

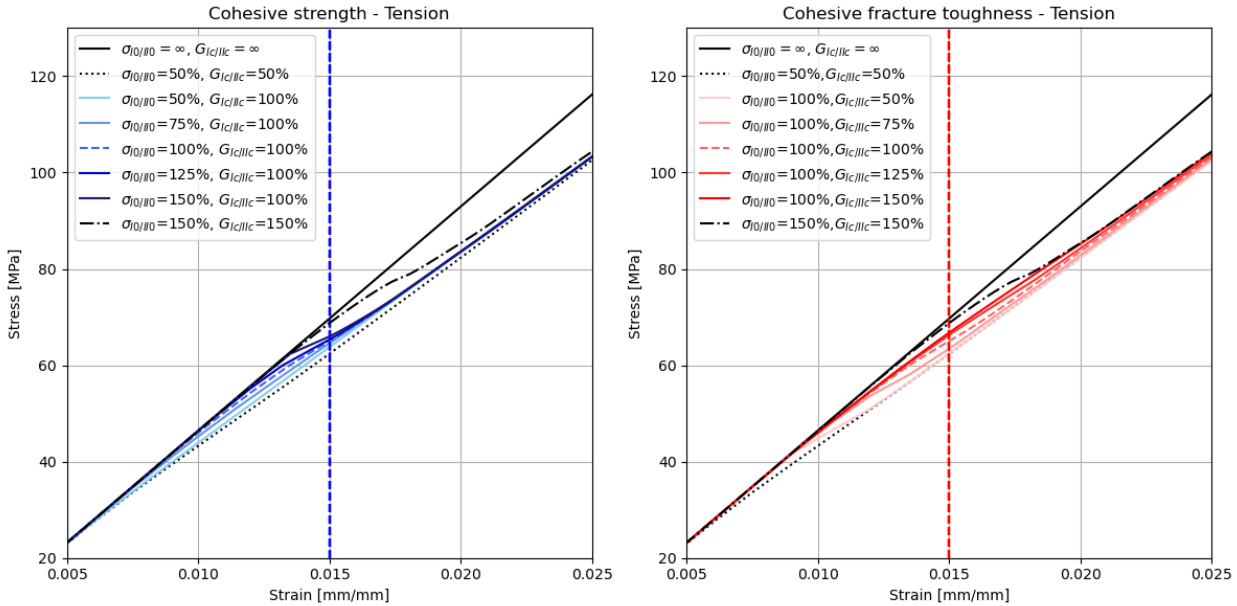

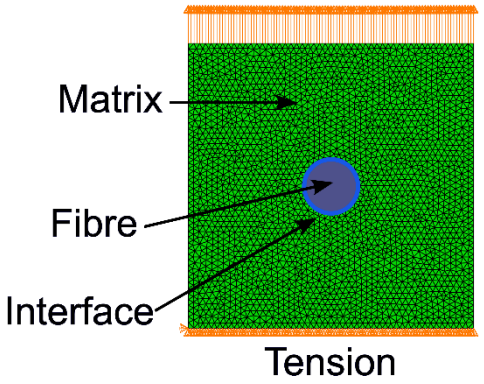

Single fibre (PF + Cohesive damage)

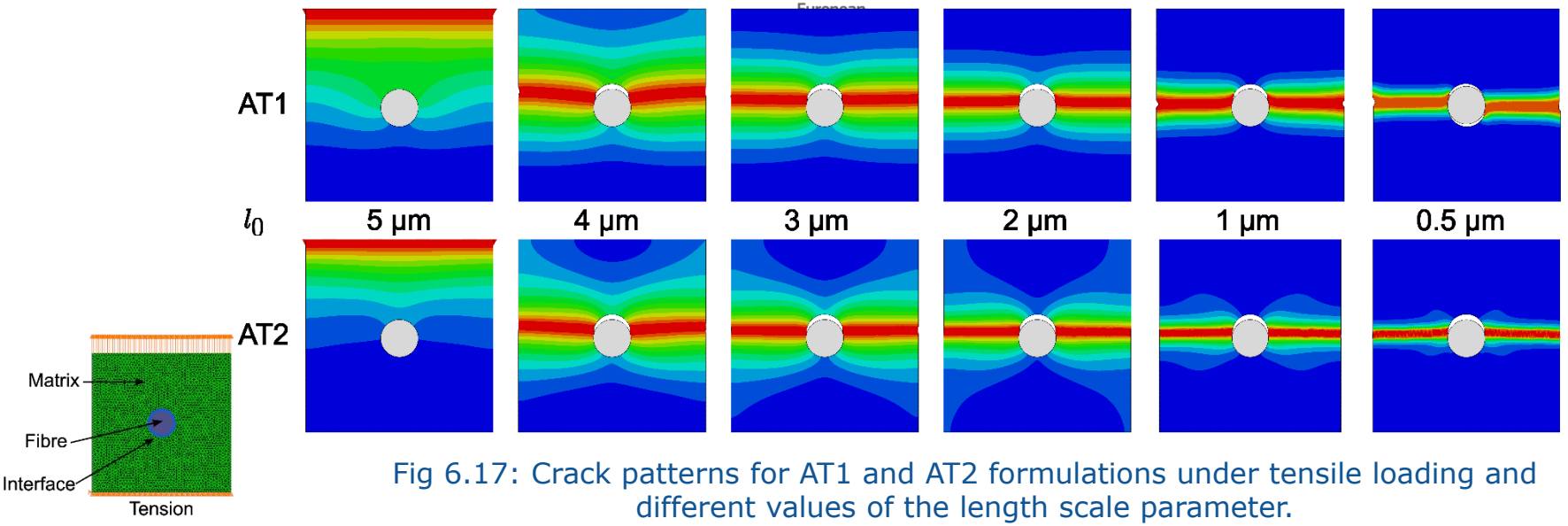

Fig 6.17: Crack patterns for AT1 and AT2 formulations under tensile loading and different values of the length scale parameter.

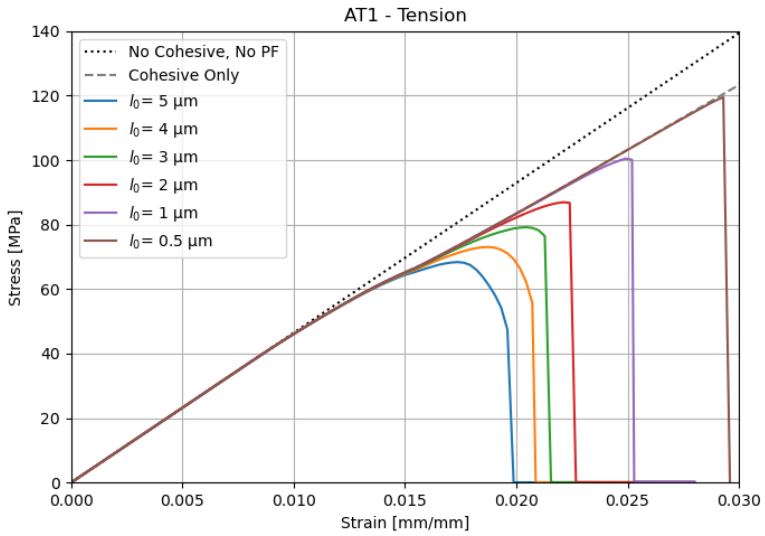

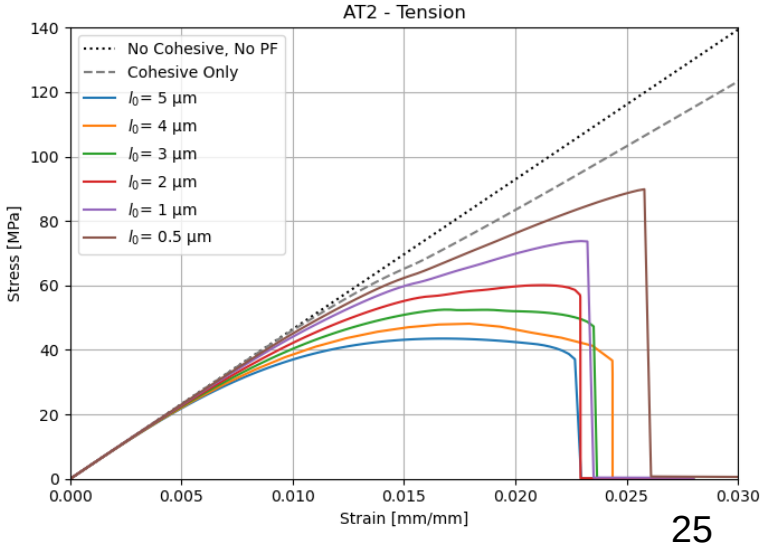

Single fibre (PF + Cohesive damage)

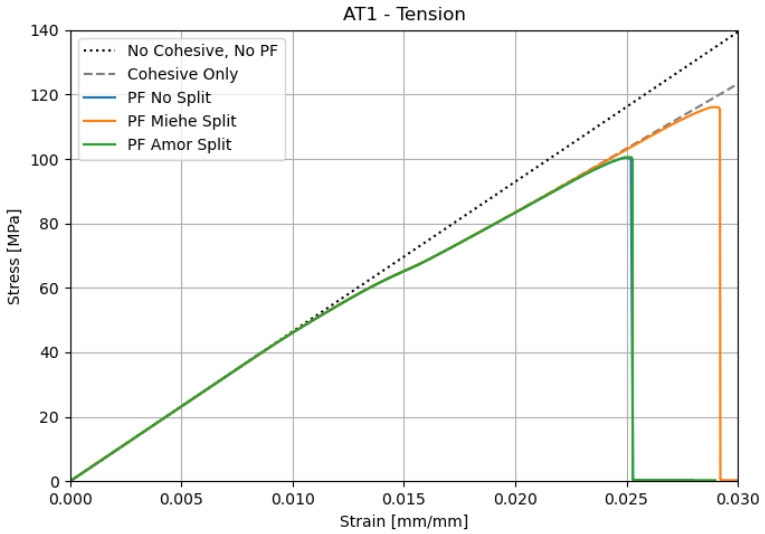

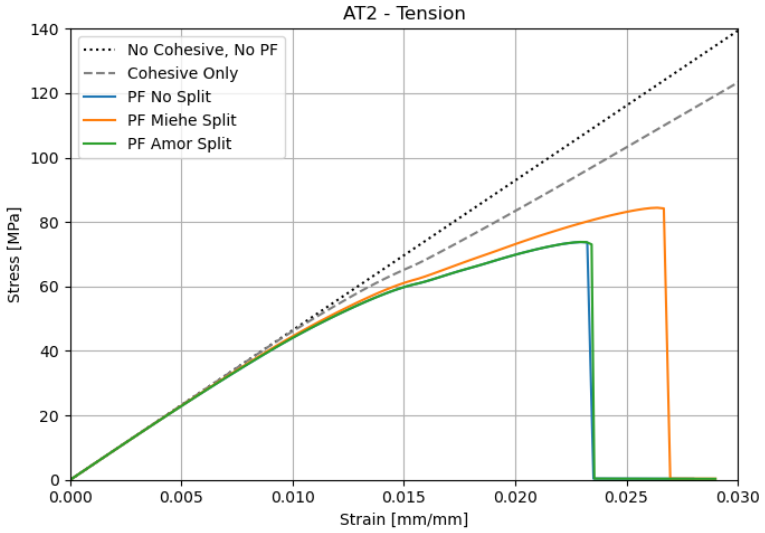

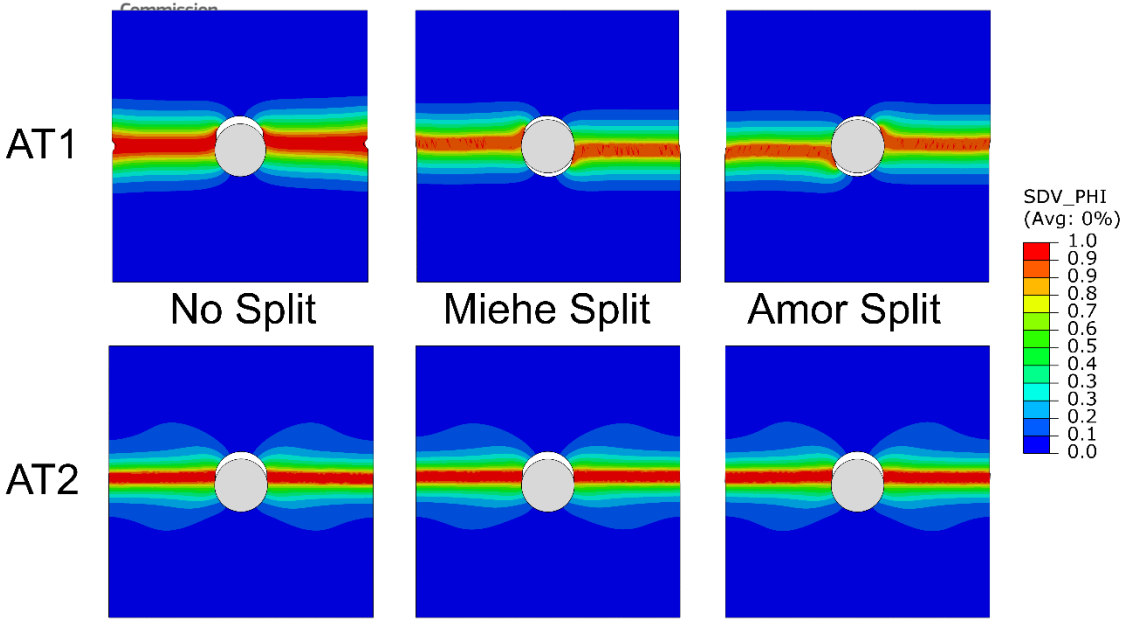

Fig 6.23: Crack patterns for AT1 and AT2 formulations under tensile loading and different energy splits.

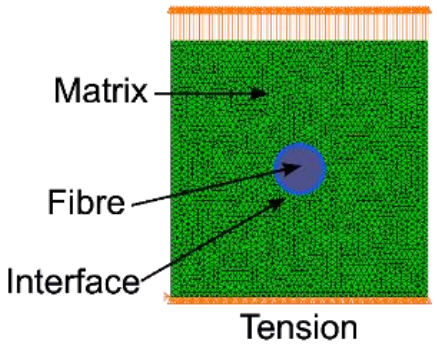

European Commission

RVE analysis

Research Executive Agency

RVE (Cohesive damage)

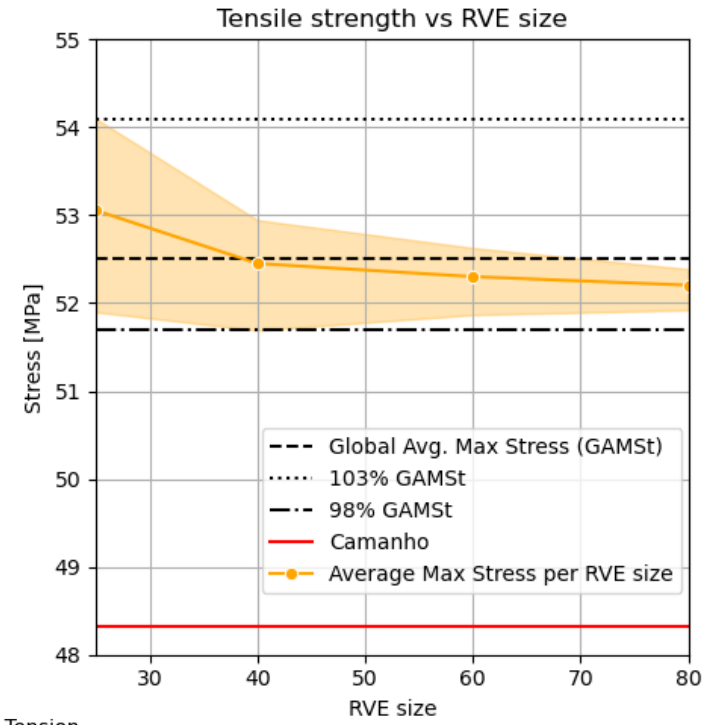

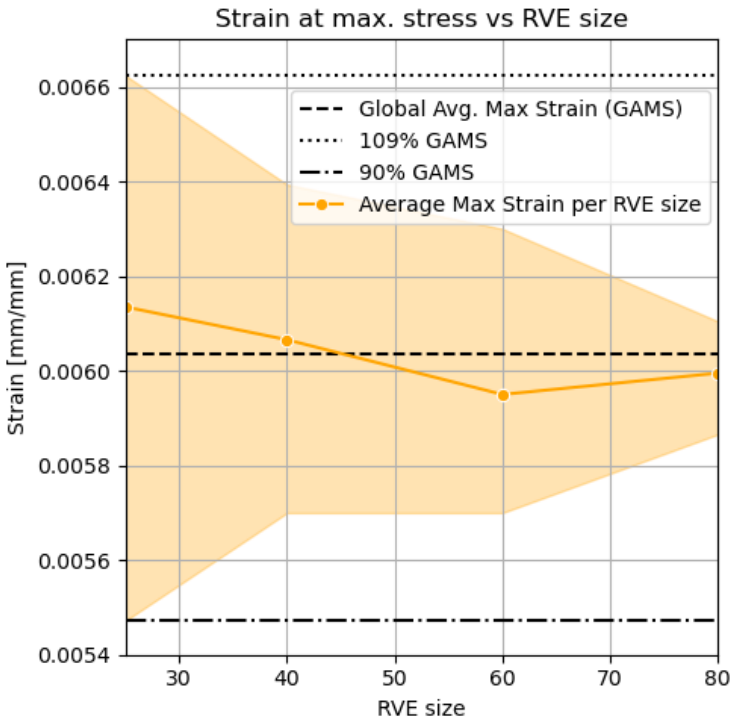

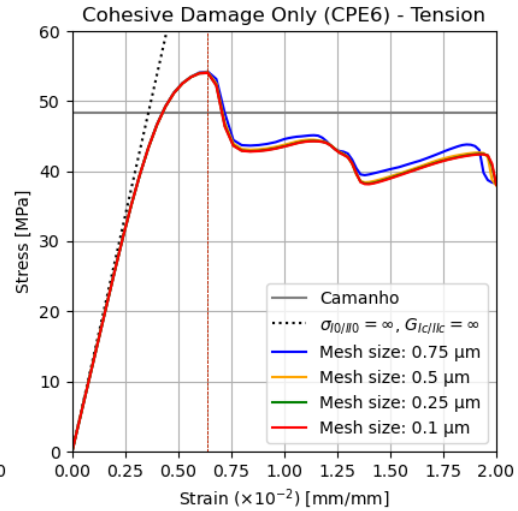

Fig 7.5: Evolution of tensile strength and strain at maximum tensile stress for different RVE sizes.

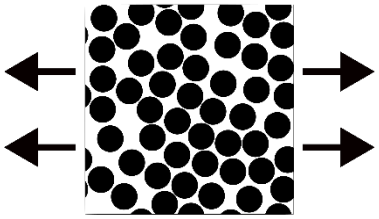

Tension

RVE (Cohesive damage)

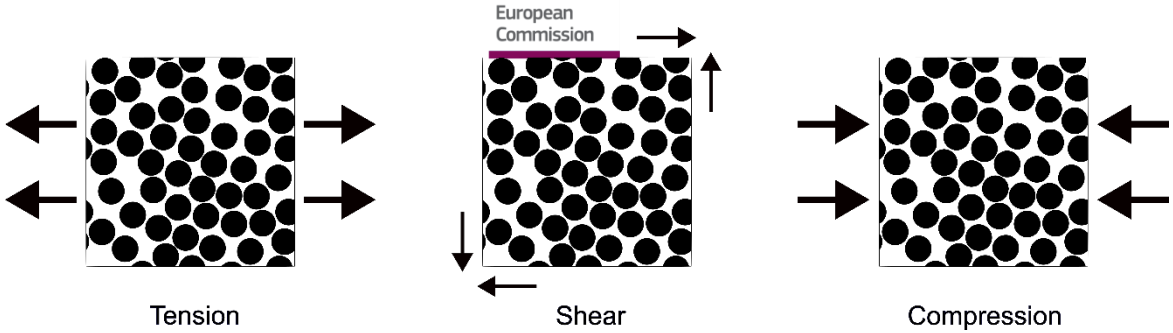

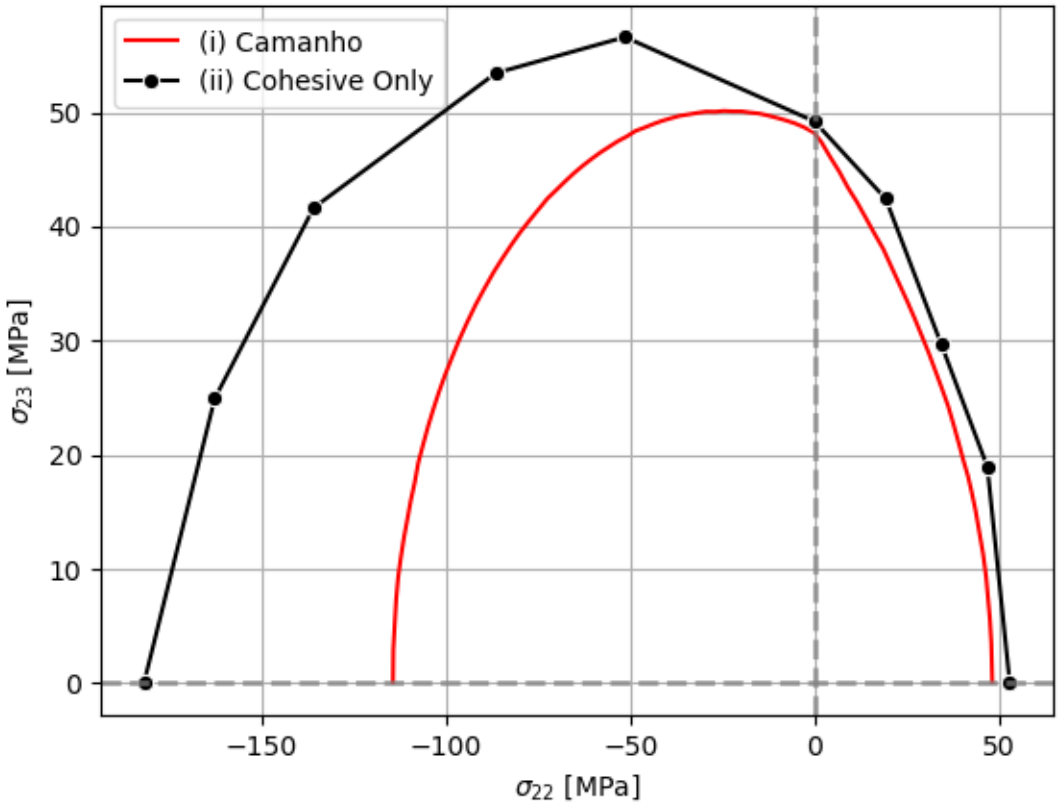

Fig 7.8: Failure envelopes of: (i) Camanho et al. [18] and (ii) linear-elastic matrix and cohesive interface damage (Cohesive Only).

RVE
(PF + Cohesive damage)

European Commission

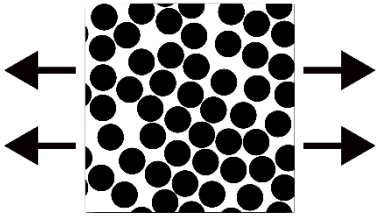

Fig 7.15: Maximum, minimum, average and standard deviation of (a) the peak stress values and (b) the strains at peak stress for different RVE sizes under tensile loading, Phase-Field AT1 formulation and Miehe's energy split.

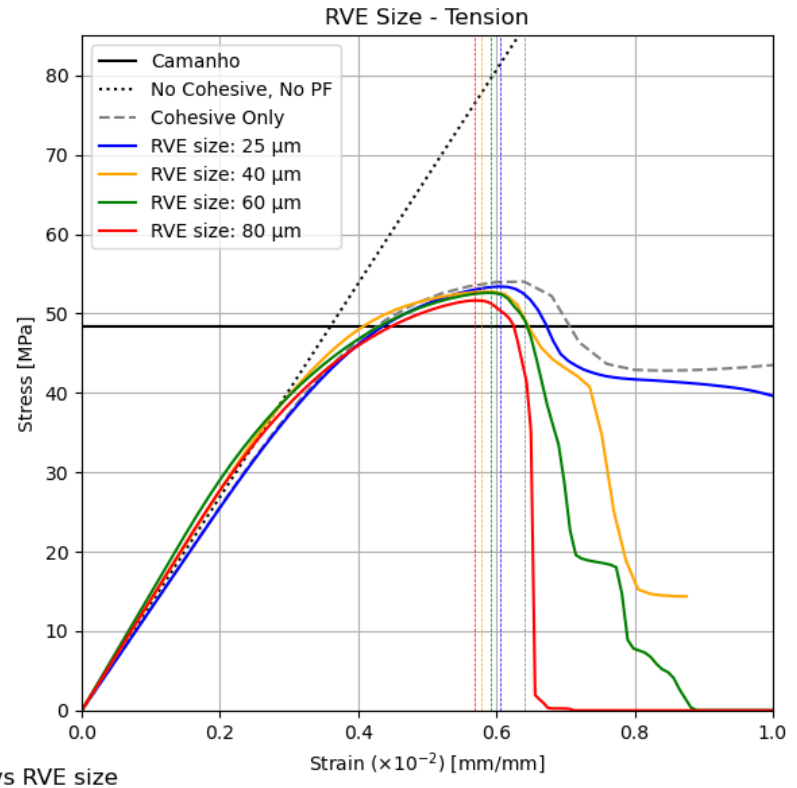

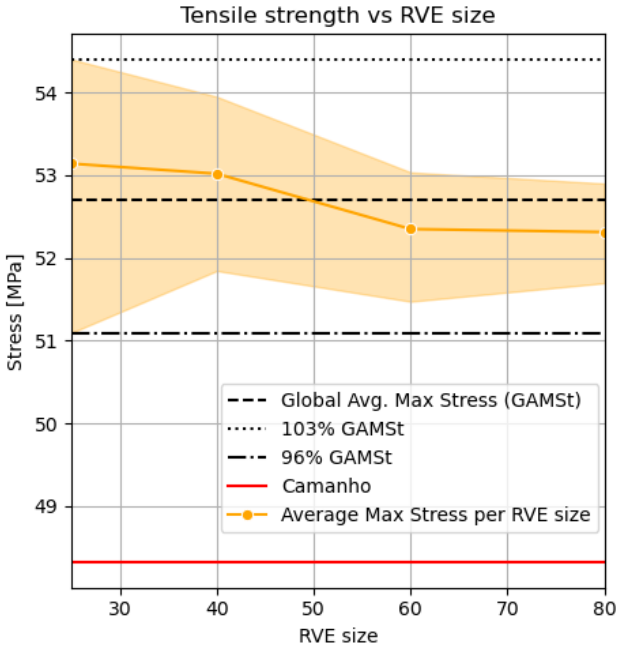

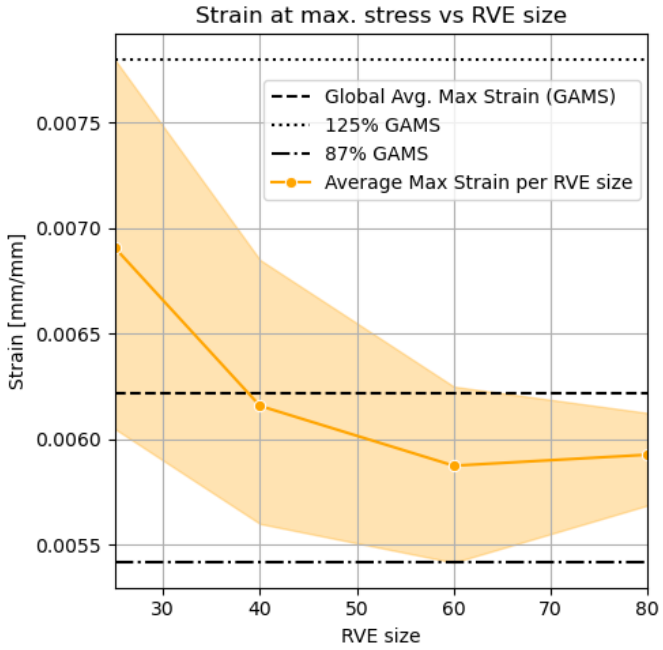

Fig 7.18: Stress-strain curves for a perfect interface connection (No Cohesive, No PF) compared to a model considering a damageable cohesive interface only (Cohesive Only) and models considering cohesive and PF damage using the AT1 formulation and Miehe's energy split. Different RVE sizes were used for tensile loading.

RVE
(PF + Cohesive damage)

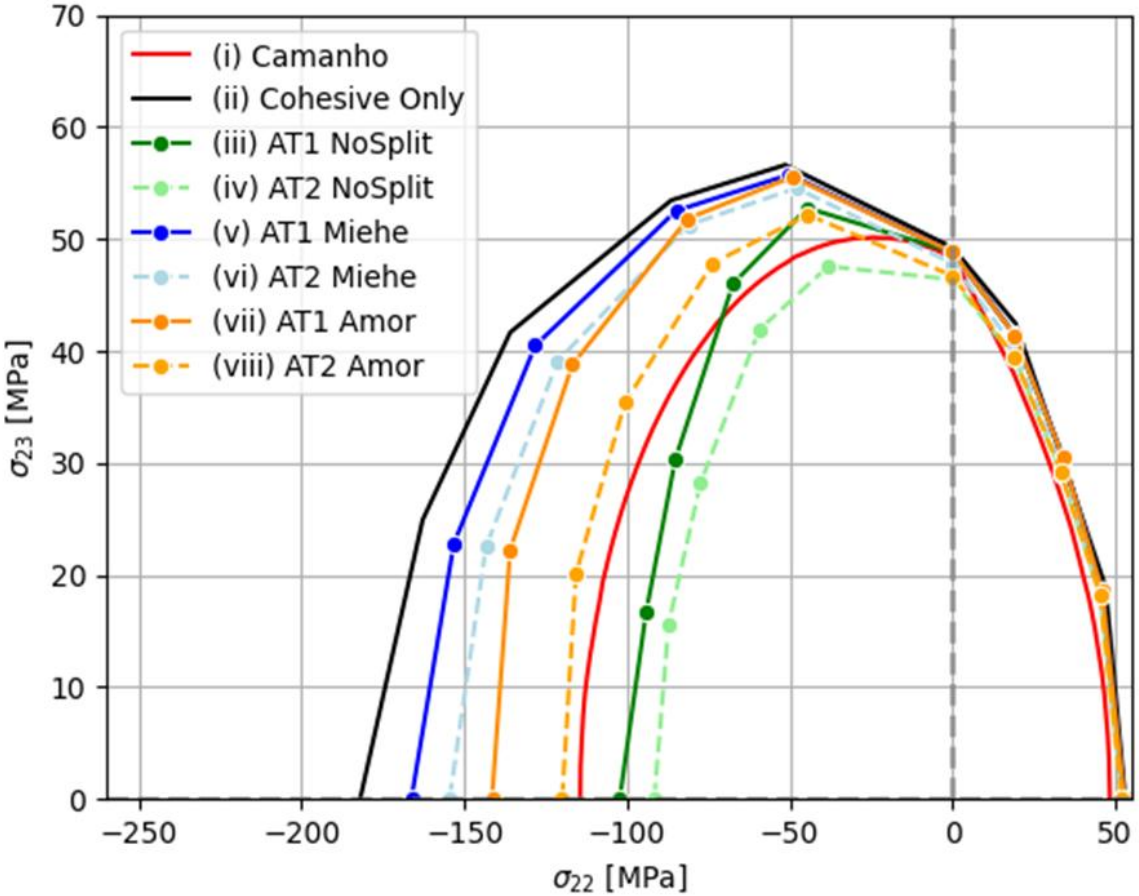

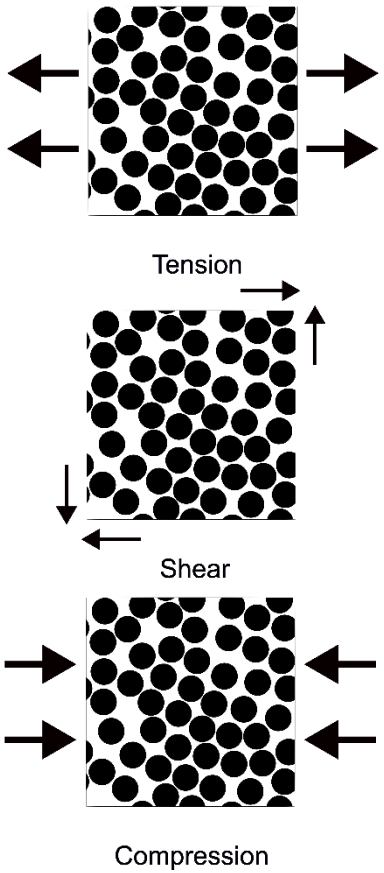

Fig 7.23: Failure envelopes of: (i) Camanho et al. [18] and (ii) linear-elastic matrix and co hesive interface damage (Cohesive Only), (iii) AT1 No Split, (iv) AT2 No Split, (v) AT1 Miehe's split, (vi) AT2 Miehe's split, (vii) AT1 Amor's split and (viii) AT2 Amor's split.

RVE
(PF + Cohesive damage)

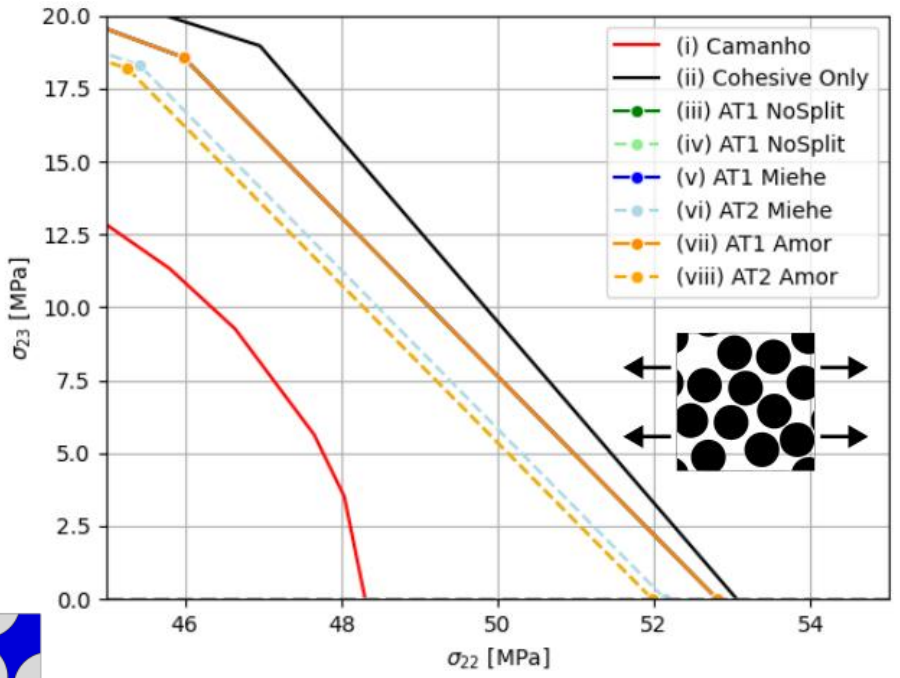

Fig 7.24: a) Failure envelopes and b) crack patterns for pure tensile load of: (i) Camanho et al. [18] and (ii) linear-elastic matrix and cohesive interface damage (Cohesive Only), (iii) linear-elastic AT1 formulation without energy split, (iv) linear-elastic AT2 formulation without energy split, (v) linear-elastic AT1 formulation with Miehe's energy split, (vi) linear-elastic AT2 formulation with Miehe's energy split, (vii) linear-elastic AT1 formulation with Amor's energy split and (viii) linear-elastic AT2 formulation with Amor's energy split

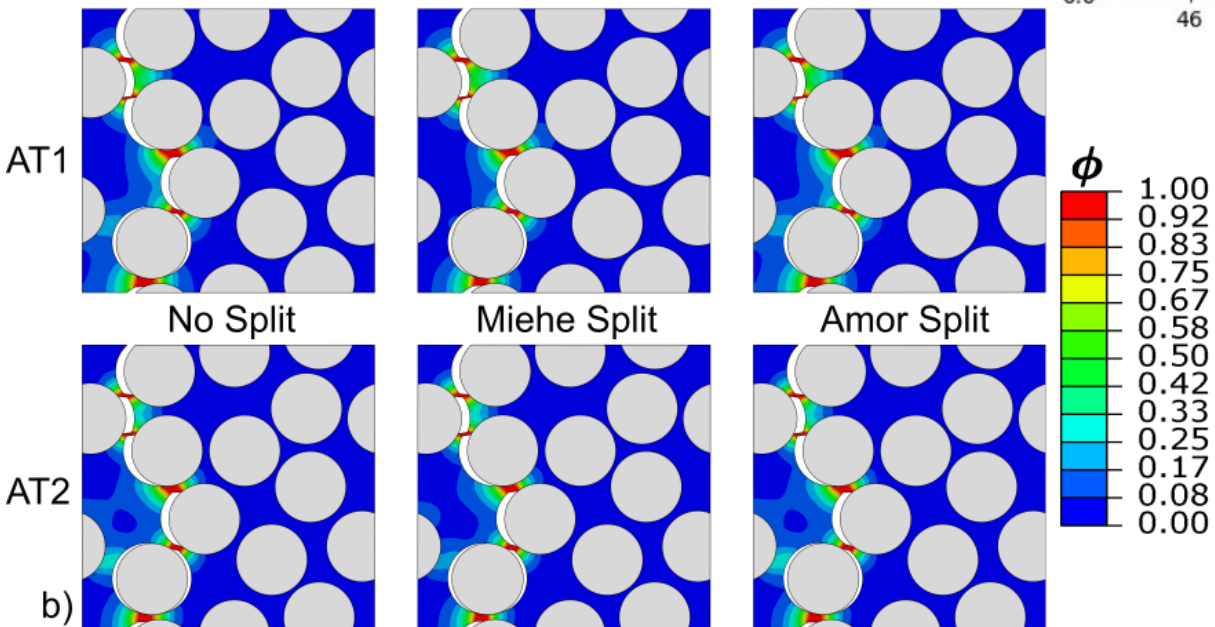

RVE
(PF + Cohesive damage)

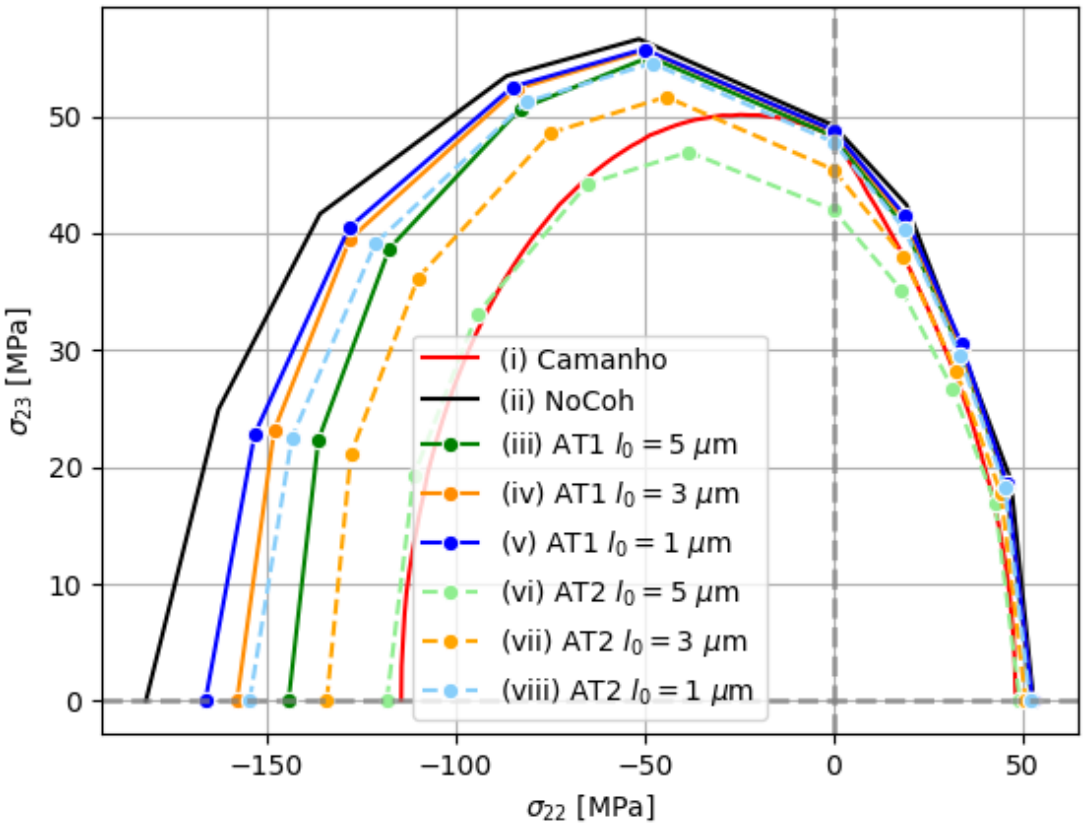

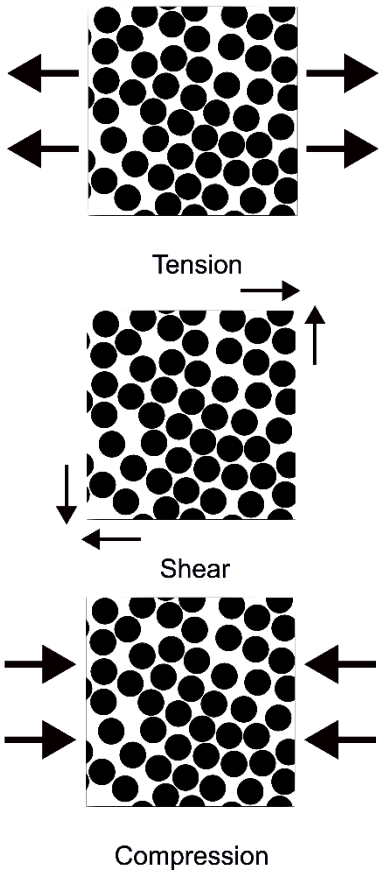

Fig 7.27: Failure envelopes computed using: (i) Camanho et al. [18], (ii) linear-elastic matrix and cohesive interface damage (Cohesive Only). AT1 and Miehe's split formulation with length scale (l0) equal to (iii) 5 μm, (iv) 3 μm and (v) 1 μm. AT2 and Miehe's split formulation with length scale equal to (vi) 5 μm, (vii) 3 μm and (viii) 1 μm.

RVE (PF + Cohesive damage)

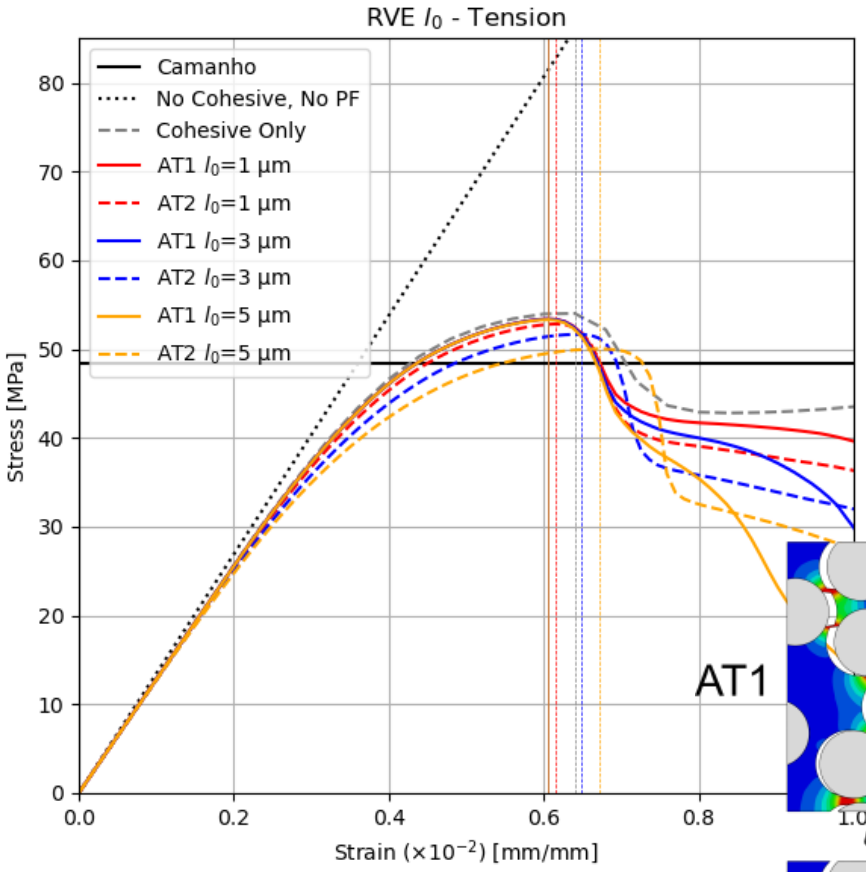

Fig 7.28: Stress-strain curves for tensile loading comparing: (i) strength according to Camanho et al. [18], (ii) RVE with perfect interface connection (No Cohesive, No PF), (iii) RVE with linear elastic materials and damageable interface (Cohesive only), (iv) RVE with PF damage using Miehe's split, AT1 formulation and $l_0 = 1$, (v) RVE with PF damage using Miehe's split, AT2 formulation and $l_0 = 1$, (vi) RVE with PF damage using Miehe's split, AT1 formulation and $l_0 = 3$, (vii) RVE with PF damage using Miehe's split, AT2 formulation and $l_0 = 3$, (viii) RVE with PF damage using Miehe's split, AT1 formulation and $l_0 = 5$, and (ix) RVE with PF damage using Miehe's split, AT12 formulation and $l_0 = 5$. μm,

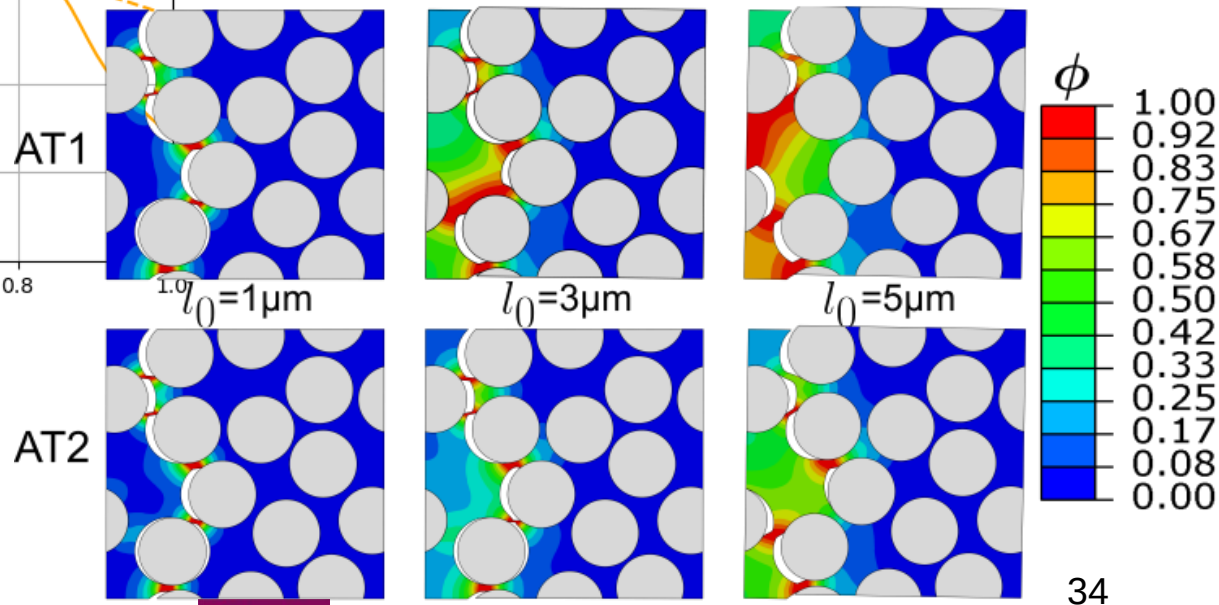

Fig 7.29: Crack patterns for tensile loading using AT1 and AT2 formulations with length scale equal to: (i) 1 μm, (ii) 3 μm and (iii) 3 μm.

Embedded cell models

Fracture in cross-ply laminates

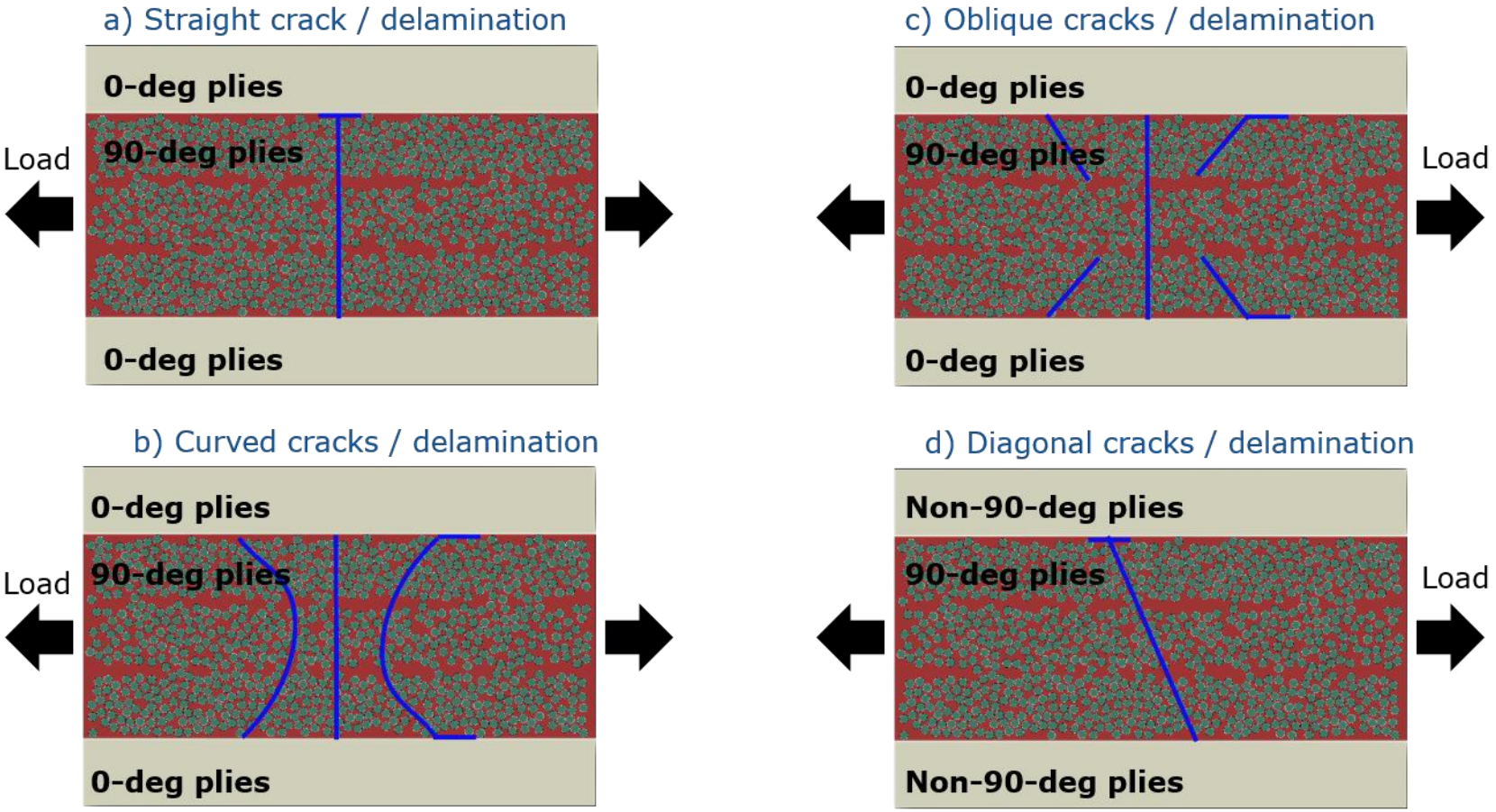

Fig 8.1: Types of transverse fracture in [(S)/90n]s laminates: a) Straight transverse crack with /without partial delamination, b) Curved cracks around a straight transverse crack with/without partial delamination, c) Oblique cracks around a straight transverse crack with/without partial delamination, and d) diagonal crack with/without partial delamination [19].

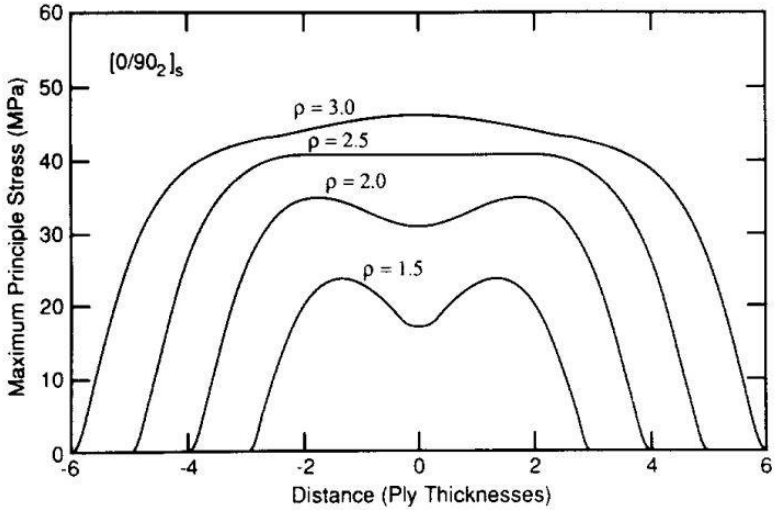

Fig 8.3: The first principal stress along the 0/90 interface in a typical [0/90]s carbon/epoxy laminate for four values of microcrack spacing, ρ is a dimensionless microcrack spacing [21].

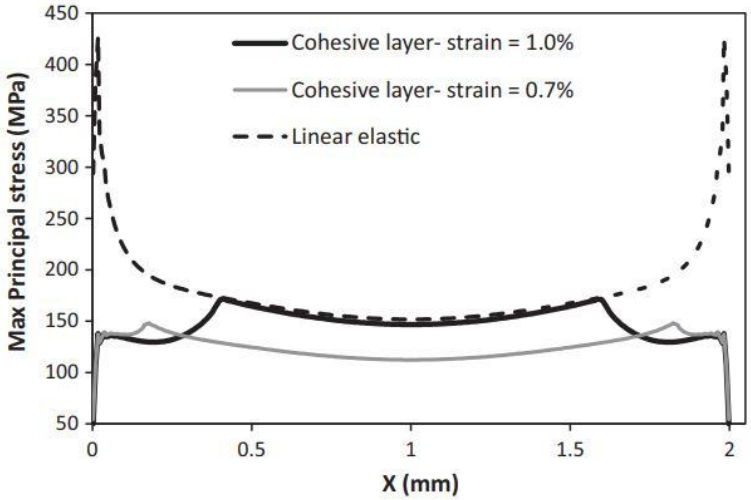

Fig 8.4: Maximum principal stress (S1) at the 0/90 interface [20] with cohesive elements at the interface at 1% longitudinal deformation (Cohesive layer- strain = 1.0%), with cohesive elements at the interface at 0.7% longitudinal deformation (Cohesive layer- strain = 0.7%) and using a tie constraint at the interface (Linear elastic).

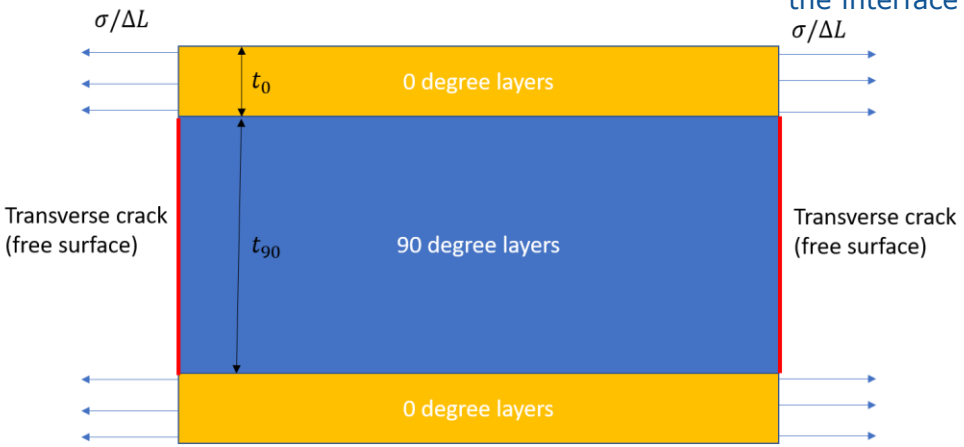

Fig 8.2: Traditional modelling approach to study transverse fracture [20, 21].

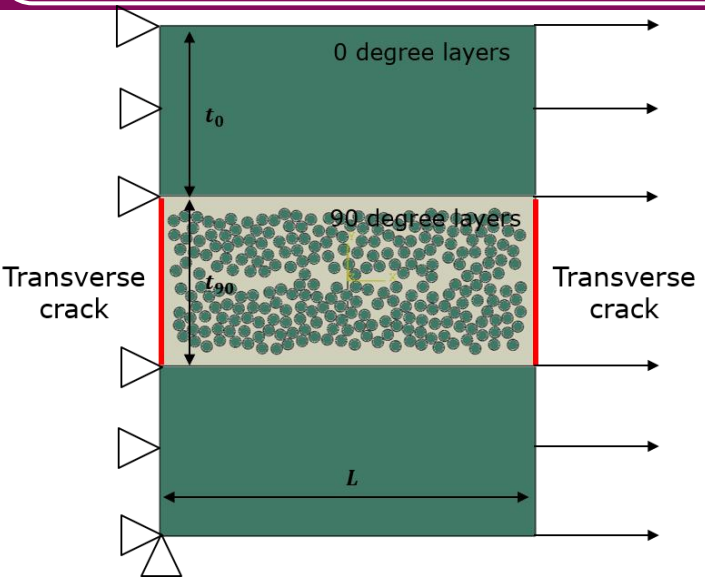

Fig 8.9: Micro-scale embedded section in a cross-ply laminate. Boundary conditions and model explanation.

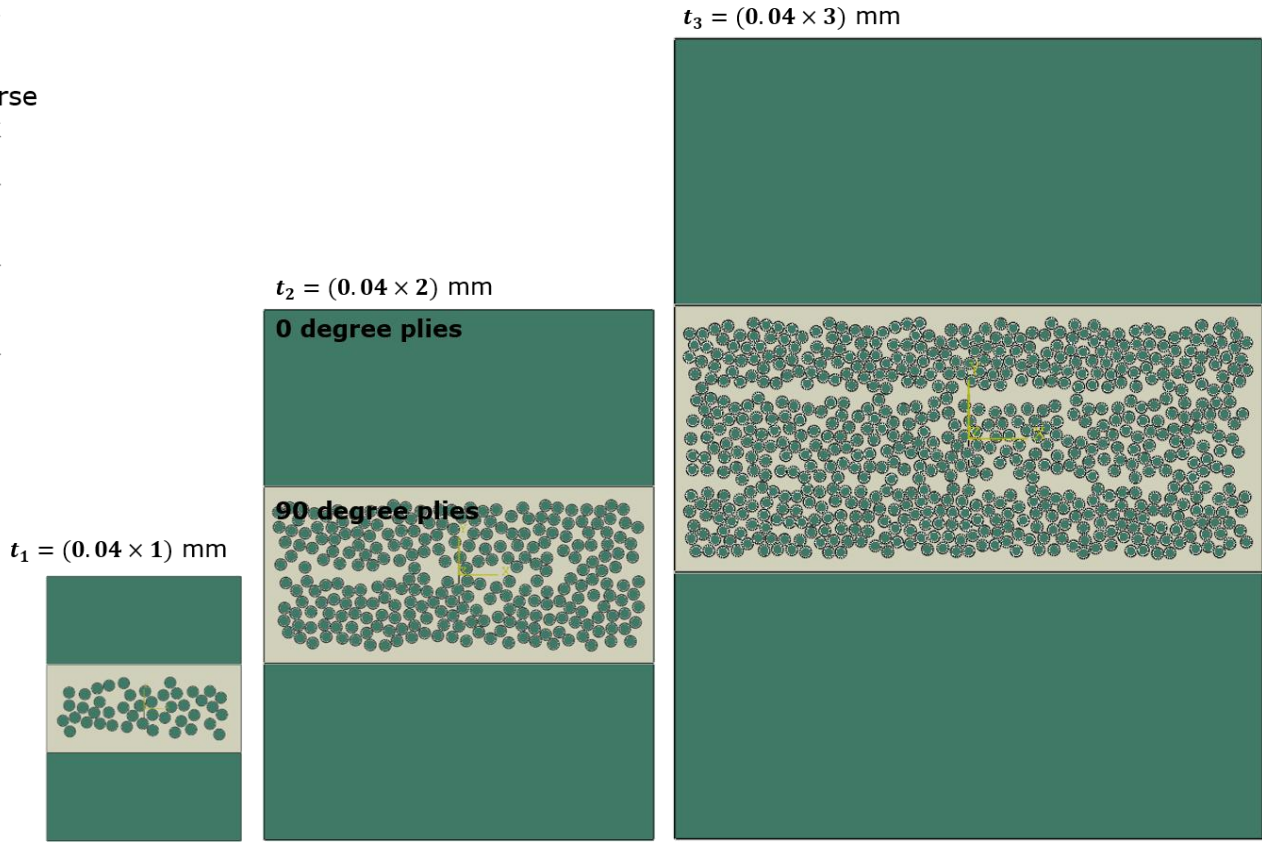

Fig 8.10: Micro-scale embedded sections in cross-ply laminates. Fibre distributions for different ply thicknesses.

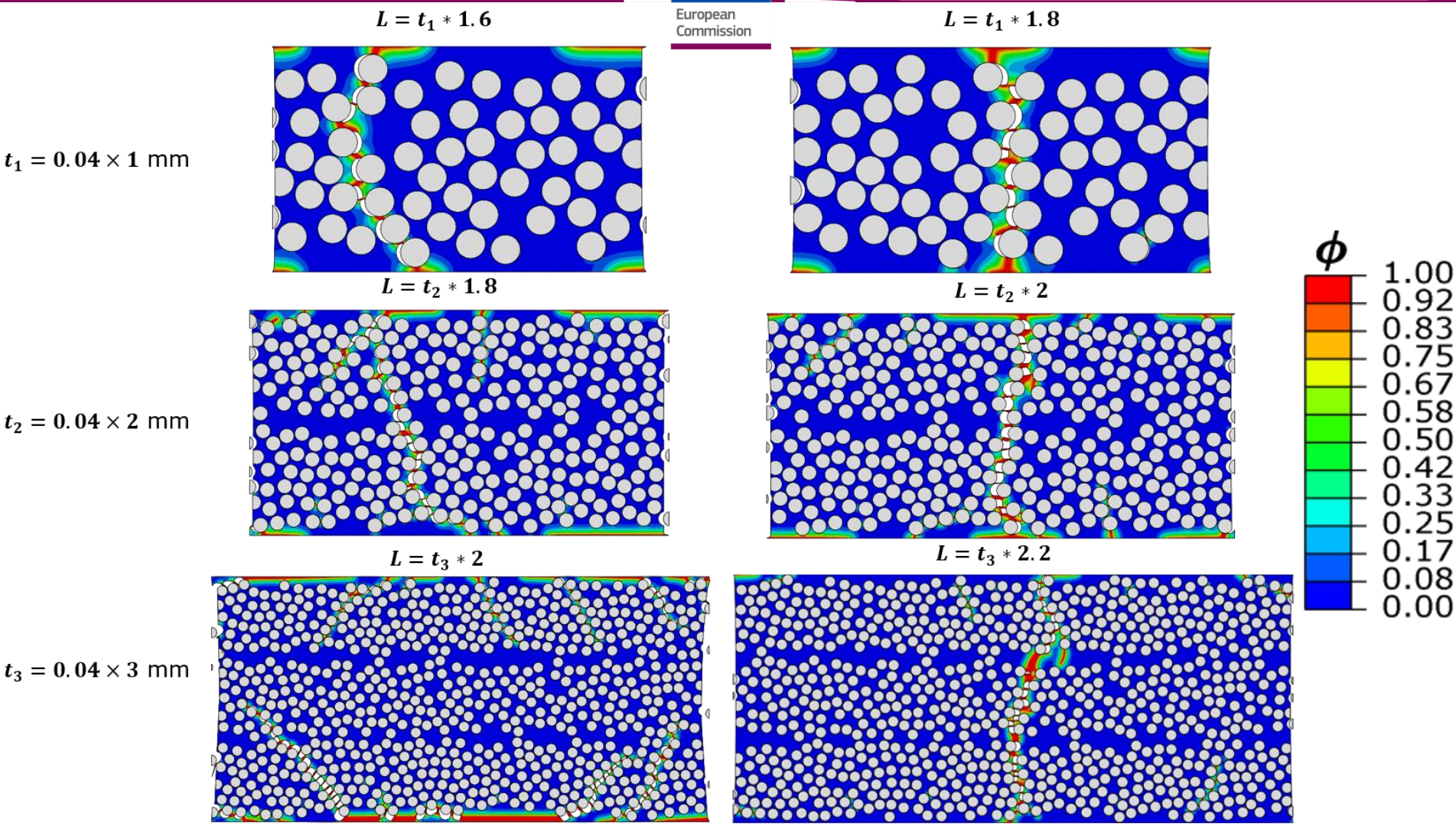

Fig 8.11: PF damage and cohesive interface separation in the micro-scale embedded sections in cross-ply laminates of different normalised lengths and thicknesses. The results in the left-hand side show the formation of curved or oblique cracks, while the results on the right-hand side show the formation of a straight transverse crack.

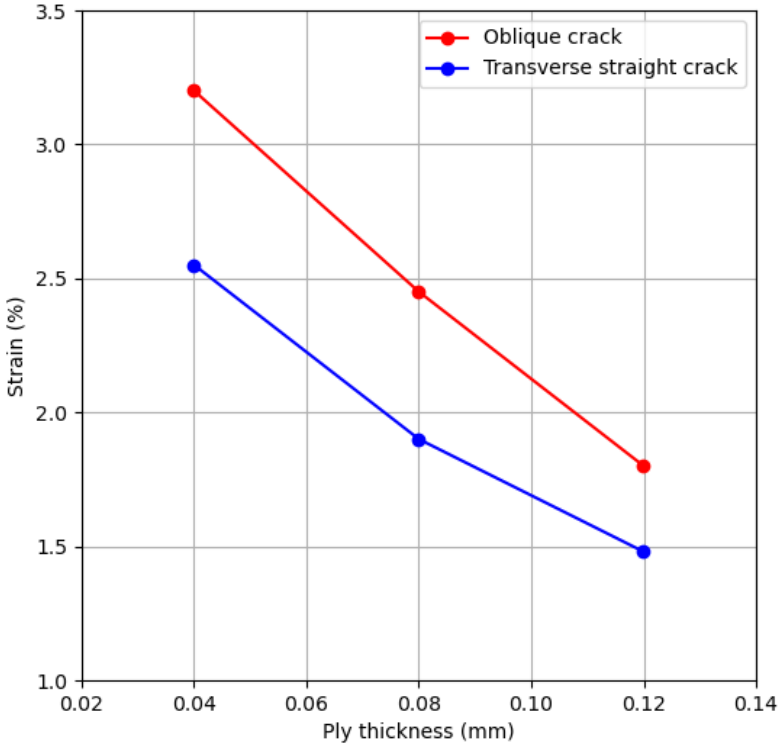

Figure 8.12: Maximum strain to create and oblique or transverse straight crack in layups of different thickness.

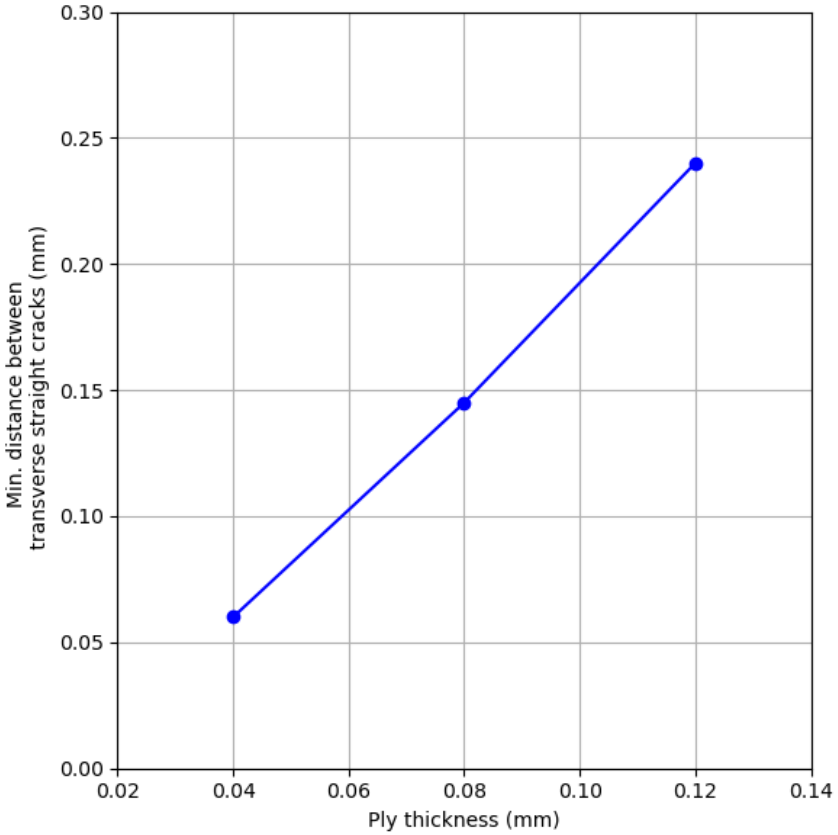

Fig 8.13: Minimum absolute distance between transverse cracks necessary to observe an oblique crack as a function of different inner layer thicknesses.

$t_3 = 0.04 \times 3$ mm

$L = t_3 * 2$

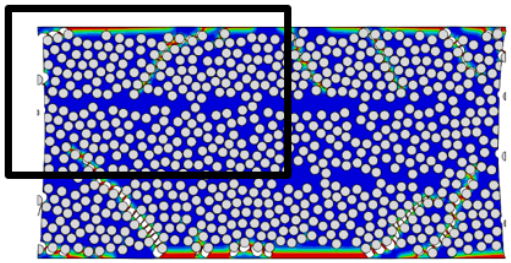

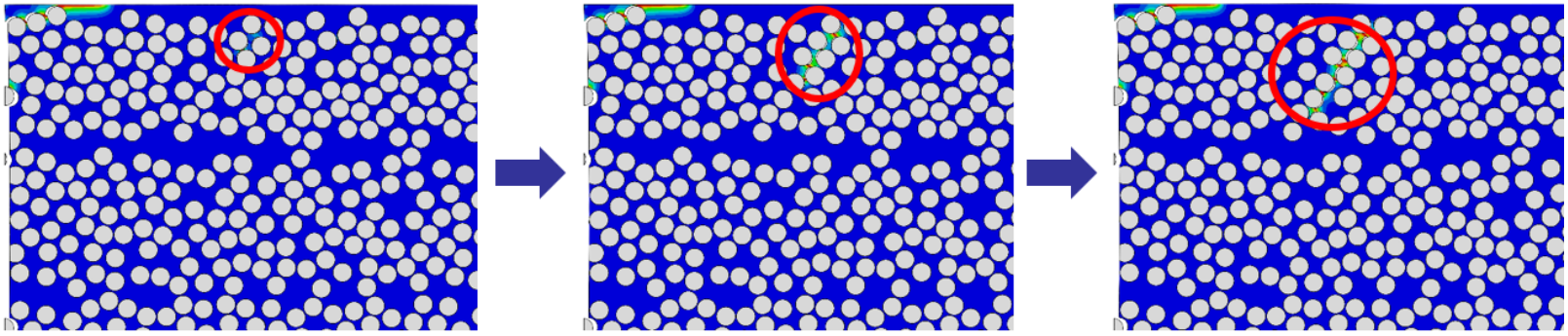

Strain = 1.6 %

Strain = 1.7 %

Strain = 1.8 %

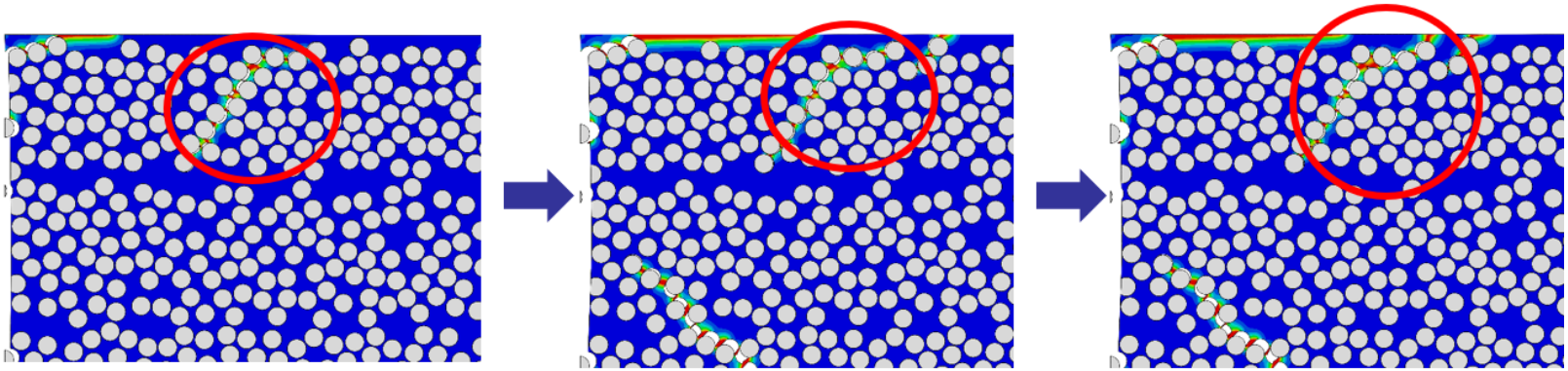

Strain = 2.1 %

Strain = 2.9 %

Strain = 3 %

Fig 8.14: Evolution of the upper left oblique crack in the representative section of the layup t_3 =0.04×3 mm, $L = t_3 \times 2$.

Conclusions and future work

Conclusions and future work

European Commission

Key Challenges & Knowledge Gaps

- **Experimental Limitations**: Micro-scale strain measurement techniques are unreliable.
- **Material Variability**: Inconsistent material property values create challenges.
- **Fibre-Matrix Interactions**: Fracture behaviour depends on fibre-matrix strength, but interface properties are very difficult to measure.
- **Validation Issues**: Lack of reliable experimental benchmarks limits numerical model validation.

Implementation in Abaqus: UEL vs. UMAT

- **UEL (User Element)**: Better numerical performance, but difficult post-processing.
- **UMAT (User Material)**: Easier visualization but less computational flexibility.
- **Key Insight**: The choice depends on balancing computational efficiency with analysis depth.

Role of Boundary Conditions & RVE Size

- Boundary conditions significantly impact fracture predictions, especially in localized failure.
- Fibre distribution & RVE loading introduce variability.
- Need for systematic guidelines to select appropriate conditions.

Conclusions and future work

European Commission

RVE & Embedded Cell Model Insights

•Fibre distribution, resin thickness, and RVE/cell size significantly affect fracture predictions.

•Traditional PF models play a minor role under **tensile-dominated loading.** The influence of PF parameters becomes more relevant for **compressive and shear loading**.

•The large amount of material, interface and model parameters can be adapted to fit the target/validation data. However, this does not warrant an accurate approach.

Recommendations & Future Research

•**Improve Experimental Techniques**: Reduce artefacts & enhance strain measurement accuracy.

•**Enhance Numerical Approaches**: Systematic parameter selection & transparent methodologies.

•**Develop Advanced Models**:

- Integrate elasto-plastic & hyper-elasto-plastic formulations with PF.
- Explore alternative PF models with micro-scale length scale can be defined independent of mechanical properties.

Conclusion

•The **Phase-Field method** has strong potential for fracture modeling but requires further development.

•Bridging experimental & numerical research is **critical** for improving composite material design & reliability.

European Commission

Thank you!

Research Executive Agency